All-Optical Switching in Silicon Microspheres

by

Farhan Azeem

A Thesis Submitted to the
Graduate School of Sciences and Engineering
in Partial Fulfillment of the Requirements for
the Degree of

Master of Science

in

Optoelectronics and Photonics Engineering

Koç University

September 2015

Koç University

Graduate School of Sciences and Engineering

This is to certify that I have examined this copy of a master's thesis by

Farhan Azeem

and have found that it is complete and satisfactory in all respects,
and that any and all revisions required by the final
examining committee have been made.

Committee Members:

____

Ali Serpengüzel, Ph. D. (Advisor)

____

Erdem Alaca, Ph. D.

____

Erdal Bulğan, Ph. D.

Date: ______________________

ABSTRACT

Silicon is a cheap and naturally abundant material and has contributed to the electronics revolution, which in turn has led to the foundation of separate fields known as silicon electronics and silicon photonics. In silicon photonics optical resonances are utilized, which are useful for various applications, i.e., optical components such as Fabry-Pérot resonators. However, with the passage of time focus has shifted to three dimensional optical resonators with microspheres being the prime example. Nowadays, optical resonances excited in microspheres are called whispering gallery modes (WGMs) and they can be beneficial for various photonics applications. In this work, a silicon microsphere, with a 1 mm diameter and a refractive index of 3.48, is used to excite the WGMs of the silicon microsphere by evanescent coupling with a silica optical fiber half coupler (OFHC). A near infrared CW laser with the central wavelength of 1472 nm is used for the excitation of the WGMs. Additionally, these WGMs are tuned with the help of a pulsed 405 nm Fabry-Pérot laser, which acts as pump laser to modify the refractive index of the microsphere. As the pump energy changes, an average red shift of 0.37 nm in the WGMs spectrum of the silicon microsphere is observed for 50% duty cycle of the pump laser, which leads to a refractive index change of $\Delta N = 8.75 \times 10^{-4}$ and a temperature change of $\Delta T = 4.70$ K. This behavior can be explained by the thermo-optic effect (TOE) in silicon. All-optical switching in time domain is also carried out for the WGMs of the silicon sphere, as the pump modulates the refractive index of silicon, the resonant peaks are observed to be shifting in time domain. Overall, TOE tuning of the resonant spectra is shown to be beneficial for the all optical control of silicon resonators. This technique can be useful for applications in silicon photonics.

ÖZET

Silisyum oldukça bol bulunan ve uygun optik özellikleri olan bir gereçtir. Silisyum kullanılarak elektronik devrimi gerçekleştirilmiş ve silisyum elektronik/fotonik araştırma alanı ortaya çıkmıştır. Silisyum, fotonik alanında optik çınlamalar için de kullanılmakta olup, Fabry-Pérot çınlaçları gibi birçok optik aygıtta yer almaktadır. Silisyum fotoniğinin gelişmesi ile 3 boyutlu optik çınlaçlar önem kazanmış ve mikroyuvarlar ana araştırma dallarından biri olmuştur. Bugünlerde, mikroyuvarlarda uyarılan optik çınlamalara fısıldayan geçit kipleri (FGK) denmektedir ve bu çınlamalar birçok fotonik uygulamasında yer bulmaktadır. Bu çalışmada, 1 mm çaplı ve kırılma katsayısı 3.48 olan silisyum mikroyuvarlarda FGK'leri çalışılmıştır. Optik çınlamalar, mikroyuvarların optik dalga kılavuzlarına bağlaşması ile elde edilmiştir. Bu çalışmada, FGK'lerin uyarılması için dalgaboyu 1472 nm olan sürekli dalga kızılaltı lazer kullanılmıştır. Ek olarak, 405 nm dalga boyunda çalışan bir Fabry-Pérot lazeri sayesinde 1472 nm'de gözlemlenen FGK'lerin yönetilmesi amaçlanmıştır. 405 nm lazer, uyarı lazeri olarak kullanılarak silisyum mikroyuvarların kırılma katsayıları üzerinde ısıl-optik etki yaratılmıştır. Uyarı lazer gücünün değişmesi ile yuvar kırılma katsayısı $\Delta N = 8.75x10^{-4}$ ve yuvar sıcaklığı $\Delta T = 4.70$ K miktarında değiştirilmiş ve bu yolla FGK'ler 0.37 nm kırmızıya kaydırılmıştır. Ek olarak, mikroyuvarlarda çınlayan ışık zaman boyutunda da incelenmiş ve uyarı lazeri yuvar kırılma katsayısını değiştirdikçe FGK'lerin zaman ekseninde de kaydırıldığı gözlemlenmiştir. Yapılan çalışma, ısıl optik etki ile optik açma-kapama yönetiminin olabilirliğini göstermiş ve optik yollarla FGK'lerin yönetilebileceğini ortaya koymuştur.

ACKNOWLEDGEMENTS

I would like to thank my supervisor, Prof. Dr. Ali Serpengüzel for his guidance and support during my stay at Koç University. I am grateful to him for giving me the chance to work at his group in the Koç University Microphotonics Research Laboratory (KUMRL). I would also like to thank my committee members Assoc. Prof. Dr. Erdem Alaca, and Asst. Prof. Dr. Erdal Bulğan for their critical reading of my thesis and their constructive comments.

I would like to thank my laboratory teammates Dr. Ulaş Sabahattin Gökay for his kindness, guidance and cooperation throughout my stay in KUMRL. Rehan Chaudhry, Sohail Anwar, Hamza Humayun, Muhammad Zakwan, Zeeshan Rashid, Sultan Bukhari, and Imran Khan for their support and counsel during my stay at KUMRL. I would like to thank Dr. Sharif Murib for his intellectual input towards my thesis and research and Selçuk Çakmak for help with experimental components.

Furthermore, I would like to thank my cousins Malik Jawad, Haroon Afridi, my brother in law Humayun Afridi, and friends Mashood Alam, Arsalan Aziz, Faraz Khan, Zohaib Khan, Ahmad Khan, Qazi Uzair, Fahim Zafari, Waris Sabah, Qadir Afridi, Ibrahim Khan, Shafi Khan, Atiq Khan, Khizar Zia, Zirgham Zia, Rizwan Khan, Alamzeb Khan, Tauseef Ahmad, Rajab Ali, Mahmood Khan, Shahzad Syed, Usman Altaf, Usman Afridi, Ghulam Nabi, Talha Irfan, Joao Vitor and Fahad Sohrab for their support and encouragement during my stay abroad.

I would like to thank Doğukan Atmaca and Aziz Karaşahin, who made me feel at home during my stay in Istanbul.

I would like to thank my teachers Qari Roohullah, Shaukat sahib (late), Naveed Khan, Luqman Qadir (late) and Rehmatullah Kundi, Dr. Naveed Aman, Maqsood Khan and Dr. Omar Usman for their recommendations and support for my graduate education.

I would also like to acknowledge Türkiye Bilimsel ve Teknolojik Araştırma Kurumu (TÜBİTAK) grant No: 114F312 for the partial financial support to our research and Devlet Planlama Teşkilatı (DPT) research infrastructure grant for Koç University Surface Technologies and Applications Research Center (KUYTAM) for the scanning electron microscope (SEM) measurements.

Finally, I would thank Pakistan Higher Education Commission (HEC) for the financial support which enabled me to come here to Turkey for graduate studies.

This Thesis is dedicated to my Parents Mr. and Mrs. Muhammad Azim Afridi and my Siblings for their everlasting love and support throughout my academic life.

TABLE OF CONTENTS

LIST OF TABLES

LIST OF FIGURES

NOMENCLATURE

a	Radius of the spherical microresonator
b	Impact parameter
c	Speed of light in vacuum
C_e	Concentration of electrons
C_h	Concentration of holes
E	Applied electric field
k	Propagation vector
l	Radial mode order
m	Azimuthal mode number
$\mathrm{m_{ce}}^*$	Effective mass of the electrons
$\mathrm{m_{ch}}^*$	Effective mass of the holes
M_{sph}	Relative refractive index of the sphere
n	Polar/ Angular mode number
N_{imag}	Imaginary part of the refractive index
N_{out}	Refractive index of the medium
N_{real}	Real part of the refractive index
Q	Quality factor
r	Linear electro-optic coefficient
s	Kerr coefficient
x	Size parameter
α	Absorption coefficient
ΔN	Change in refractive index
Δx	Mode spacing as function of size parameter
$\Delta\alpha$	Change in absorption coefficient
$\delta\lambda$	Shift in wavelength
$\Delta\lambda$	Mode spacing as function of wavelength
ε_o	Permittivity in vacuum
Θ	Polar angle from z-axis

θ_{inc}	Incidence angle required for TIR in sphere
λ	Wavelength of light
λ_o	Wavelength of light in vacuum
λ_{FWHM}	Linewidth of a resonance
λ_R	Resonant wavelength
μ_e	Mobility of electrons
μ_h	Mobility of holes
τ	Photon lifetime in cavity
ω	Angular frequency

Chapter 1

INTRODUCTION

Elastic light scattering is one of the basic methods used for determining the optoelectronic properties of resonators of different shapes. In elastic light scattering, the photon energy remains conserved after the coupling between the incident ray of light and the optical resonator.

A common example of elastic scattering is Rayleigh scattering, the optical modes or optical resonances are analogous to the acoustic whispering gallery modes (WGMs), which were first proposed by Lord Rayleigh [1], while Gustav Mie was the first to present scattering theory for a spherical shaped object [2].

Recently, research in optical microresonators has intensified, and extensive research has been done on the subject of microresonators [3,4,5,6,7]. Microresonators of different shapes are used such as microslabs, e.g., Fabry-Pérots [8], microcylinders [9], microdisks [10], microrings [11,12], microtoroids [13], microspheres [14], and photonic crystal microcavities [15] in order to localize light, while multiple studies are performed on deformed spheres, and axisymmetric spheroid resonators [16,17]. Microresonators of different materials, such as silica [18], fused silica [19], chalcogenides [20], germanium [21], silicon [22] and are used for various applications such as optical communication [23], biosensing [24], detection [25], optical modulation [26], photonic integration, and wavelength division multiplexing (WDM) [27].

Silicon technology has grown rapidly during the past half-century, with the main application being in microelectronics. Moore's law has continued to hold true for fifty years, and silicon has been an essential component in the growth of the complementary metal oxide semiconductor (CMOS) industry [28]. However, with arrival of the new millennium, the tide has turned and semiconductor devices are swiftly approaching performance and density saturation [29], hence silicon is now seen as a material for manufacturing optoelectronic devices, since silicon photonics is compatible with CMOS technology [30].

Silicon photonics [31] has narrowed the gap between photonics and electronics [32] by using semiconductor microresonators as the intermediary [33]. Silicon microspheres with their high quality WGMs are excellent examples of three dimensional semiconductor microresonators [34,35,36].

Many demonstrations of optical modulation have been done in the near-infrared (near-IR) region for optical microresonators by using thermo-optical, electro-optical, or all-optical techniques. Thermo-optic modulation has been demonstrated by installing a heater in the structure such as a waveguide or resonator, which heats the structure and changes its refractive index, thermo-optic modulation has been demonstrated in silicon Fabry-Pérot etalon [37,38] and a shift in wavelength was observed by heating Nd^{+3} doped silica microspheres [39]. Electro-optic modulation (EOM) is achieved by applying an electric field to the microresonator. EOM can either be electro-absorptive or electro-refractive [40], and has been demonstrated in silicon microrings [41] and silicon microspheres [42,43], while a spectral shift [44] has also been demonstrated by utilizing electro-optic excitation.

All-optical control, such as modulation, and switching, is usually achieved by using a light source to control another light source. A pump laser is used to control the resonances of a probe laser, which is used for excitation. All-optical modulation is either attributed to the linear one photon absorption (OPA) at low optical intensities [45,46] and to the non-linear two photon absorption (TPA) at high optical intensities [47]. OPA and TPA are induced by using a focused pump beam or a coupled pump beam, [48,49] which lead to free carrier absorption (FCA) and free carrier dispersion (FCD).

FCA and FCD are the all-optical counterparts of electro-absorption and electro-refraction, respectively [50]. FCA results in thermo-optic effect (TOE) and generation of heat in the form of phonons, and due to the high thermo-optic coefficient of silicon, which is considerably higher than that of silica and other thermo-optical materials. TOE results in a red-shift of the spectrum, and FCD results in a blue-shift of the spectrum. Due to the high thermo-optic coefficient of silicon, a red-shift is observed, after using OPA to induce TOE. However, FCD can be made the dominant process by increasing the free carrier lifetime [51]. The TOE in silicon is strong at low frequencies [52], therefore TOE overshadows the rest of the nonlinear effects at millisecond regime.

All-optical modulation has been demonstrated in different types of optical resonators such as silicon [53,54,55] and silicon nitride [56] microrings. Similarly wavelength shifts have been observed for microspheres of different materials such as silica [57], silica coated by silicon [58], and chalcogenides [59]. Here, for the very first time to our knowledge, we report all-optical switching in silicon microspheres in the near-IR by TOE induced by OPA.

Chapter 2 gives a brief introduction to spherical resonators, with emphasis on generalized Lorenz-Mie theory to describe the modes of a spherical resonator.

Chapter 3 explains the topic of optical processes in silicon by understanding optical modulation and going into subtopics of thermo-optic modulation, electro-optic modulation, and in the end the all-optical modulation, which is the essence of this work.

In chapter 4, the all-optical wavelength tuning of resonances of the silicon microsphere is explained and demonstrated with a probe laser with a wavelength in the near-IR region and a pump laser in the visible region.

Chapter 5 covers the topic of all-optical switching of the optical resonances of the silicon microsphere in time by monitoring the elastic scattering signal.

Chapter 6 is the conclusion of this work done on the silicon microsphere resonators and includes suggestions for any possible future work.

Chapter 2

SPHERICAL MICRORESONATORS

2.1. Optical Resonators

An optical resonator is the equivalent of an electronic resonant circuit in photonics or optoelectronics. The optical resonator confines light inside itself at several different resonant frequencies. Inside the optical resonator, light either reflects back and forth or circulates, without being able to escape, generally depending on the shape of the resonator used for trapping light.

There are different types of resonators, that can confine light in different dimensions such as the one dimensional Fabry-Pérot [8], the two dimensional microtoroid [13], microring [11,12], and microdisk [10] resonators. Light can be trapped in three dimensions using a spherical resonator [14], and microspheres [44] of certain diameters and material properties.

The simplest resonator is the Fabry-Pérot resonator, which was first introduced by two French scientists Charles Fabry and Alfred Pérot in 1897 [8]. The Fabry-Pérot resonator is also called Fabry-Pérot interferometer, or the Fabry-Pérot etalon, as it was used for interferometry. Etalon is a French word, which according to Oxford English dictionary means “measuring gauge”. Fabry-Pérot etalons are mainly used in spectroscopy, laser applications and telecommunication applications. Several different types of basic resonators exist in ray and wave optics, such as the planar-mirror resonator, spherical-mirror resonator, optical fiber resonator and the ring resonator.

One of the most important uses of optical resonators is in lasers, where laser stands for "light amplification by stimulated emission of radiation". Laser itself consists of an optical resonator, which amplifies light by trapping it inside the resonator cavity and uses an amplification medium for this very purpose. However lasers also control the wavelength and the spatial distribution of light. Nowadays resonators are extensively being utilized in micro and nano-photonics to take the progressing field of optoelectronics further into the future.

2.2. Spherical Resonators

Whispering Gallery Modes (WGMs) were first illustrated by Lord Rayleigh [1], at the start of twentieth century. But Gustav Mie was the first scientist to describe the WGMs for a spherical shaped object [2]. However, it was not until the introduction of maser (microwave amplification with stimulated emission of radiation), and later laser that WGMs started to come in to the limelight and scientists looked for their applications.

The fabrication of stable optical resonators is a difficult task, however with the introduction of spherical-shaped resonators made up of dielectric material, this task was made easy, since the surface of the dielectric spherical resonator itself is responsible for trapping light by total internal reflection (TIR), which can be understood by Snell's law.

A dielectric sphere with minimal or no absorption can sustain WGMs [6], where the refractive index of a material is given by:

$$N = N_{real} + iN_{imag} \quad (2.1),$$

For a nonabsorbing material, the imaginary part of the refractive index is zero. The light stays confined inside the spherical resonator by sticking to the sides of the spherical resonator. The TIR inside a spherical resonator is illustrated in Figure 2.1, where θ_{inc} is the incidence angle of the light confined inside the resonator, N_{sph} the refractive index of the material of sphere, and a the radius.

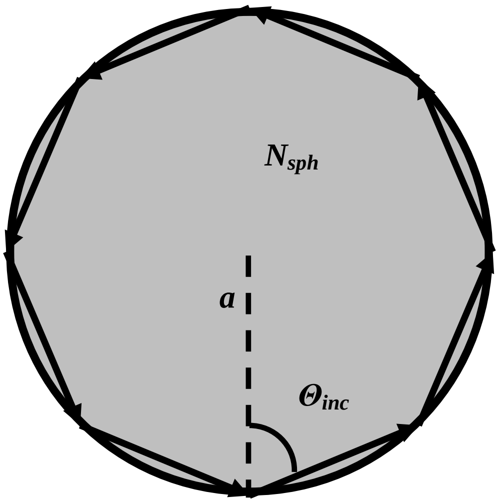

Figure 2.1: TIR inside a spherical resonator.

For the light to couple into the resonator, the resonance condition has to be met. The resonance condition for a spherical resonator is given by the following equation:

$$n\lambda_R = 2\pi a M_{sph} \quad (2.2),$$

where n is the angular mode number, a the radius, λ_R the resonant wavelength and M_{sph} the refractive index of the sphere relative to the outside refractive index. M_{sph} is given by:

$$M_{sph} = \frac{N_{sph}}{N_{out}} \quad (2.3),$$

where N_{out} is the refractive index of the surrounding medium.

2.3. Silicon Microsphere

The basis of this study is a silicon microsphere of 1 mm diameter and a refractive index of 3.48, excited with a near-infrared (near-IR) laser of central wavelength of 1472 nm. Scanning electron microscope (SEM) image of the silicon sphere is shown in figure 2.2.

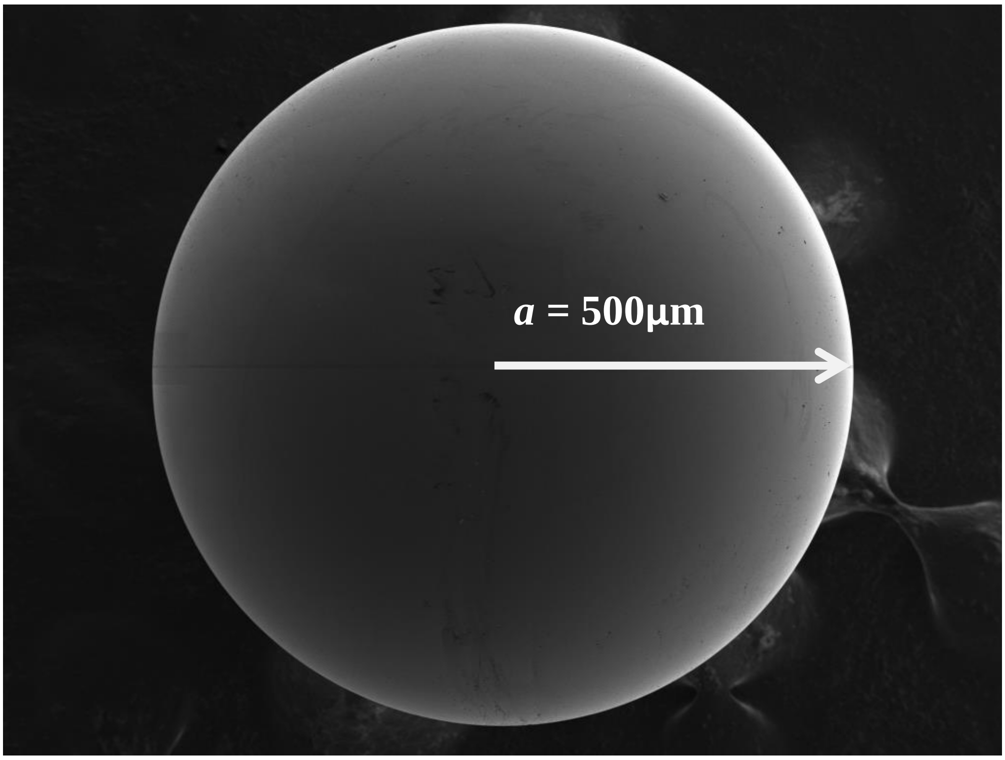

Figure 2.2: SEM image of the silicon microsphere.

Multiple studies are being performed on silicon microspheres of different sizes [22, 36, 60], such as electro-optical modulation, wavelength shifting, resonance tuning [26,42,43], while they have are also being explored for use in solar cells [61], all-optical photodiodes [62], and have possible applications in medicine [63], barcodes [64], and biosensing [65].

2.4. Whispering Gallery Modes

The WGMs of a silicon microsphere can be seen, after exciting WGMs by satisfying the resonance condition, shown in equation 2.2. However WGMs can be excited in different ways, such as plane-wave excitation or Lorenz-Mie theory (LMT) or by Gaussian-beam excitation or generalized Lorenz-Mie theory (GLMT).

WGMs occur at discrete wavelengths, and depend on the size parameter and refractive index of the microsphere. WGMs are defined by three mode numbers: azimuthal mode number (m), polar angular mode number (n), and radial mode number (l). The radial mode number shows the number of maxima in the direction of the radius, whereas the polar modes can be seen on the edges of the sphere for different angles. The azimuthal mode number describes the azimuthal distribution of the field and is degenerate with 2n+1 values, while this degeneracy can be lifted by deforming the spherical structure to that of an axisymmetric spheroid, i.e., a prolate or an oblate. Mode numbers for the resonating light inside the spherical resonator can be easily found with the solution of Equation 2.2, i.e., the resonance condition.

To observe the modes of a silicon microsphere, a finite-difference time domain (FDTD) method using electromagnetic simulation was performed by coupling a silicon microdisk resonator of 5 µm radius to a silica slab, and diamond slab waveguides of 0.5 µm width, to observe the modes of a silicon microsphere coupled to an optical fiber in two dimensions [66, 67].

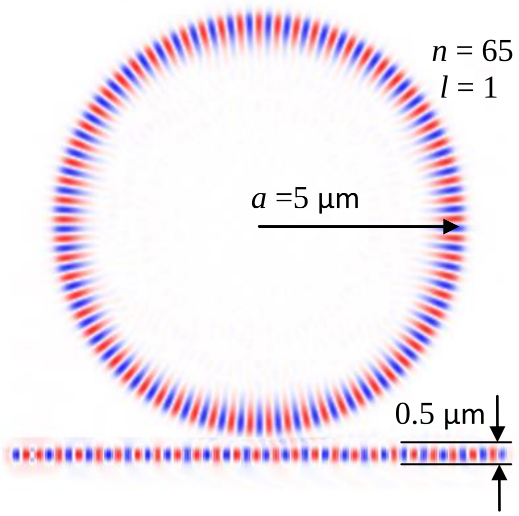

Figure 2.3: WGMs inside a silicon microdisk coupled to a silica slab waveguide.

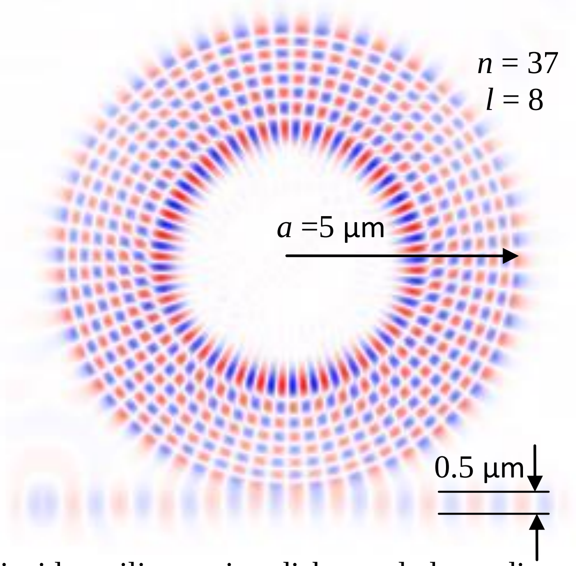

Figure 2.4: WGMs inside a silicon microdisk coupled to a diamond slab waveguide.

For figure 2.3 angular mode number is n = 65 and radial mode order is l = 1. Whereas the angular mode number is n = 37 and radial mode order is l = 8.

2.4.1. Lorenz-Mie Theory

In 1908, two physicists namely Gustav Mie and Ludvig Lorenz from Germany and Denmark, respectively proposed the theory of light scattering from a dielectric sphere, [2] and nowadays it is referred to as the Lorenz-Mie theory (LMT). LMT gives us the light scattering results of a spherical structure being illuminated with a plane wave, or in other words gives us the scattering results of a sphere by plane-wave excitation.

In LMT the incident wave is expanded into vector spherical harmonics and the expansion coefficients of the scattered field are calculated by applying the boundary conditions to the surface of the sphere. The WGMs do not occur for a single wavelength, but for a wavelength range, and the WGMs can occur in between the following boundary.

$$x < n < xM_{sph} \quad (2.4),$$

where x is the size parameter and is given by the following equation:

$$x = ka \quad (2.5),$$

where k is the wave propagation vector given by:

$$k = \frac{2\pi N_{out}}{\lambda} \quad (2.6),$$

The mode-spacing in terms of size parameter is given by the following equation [68]:

$$\Delta x = \frac{\arctan\sqrt{{M_{sph}}^2 - 1}}{\sqrt{{M_{sph}}^2 - 1}} \quad (2.7),$$

The geometry for the plane-wave excitation is shown is figure 2.5.

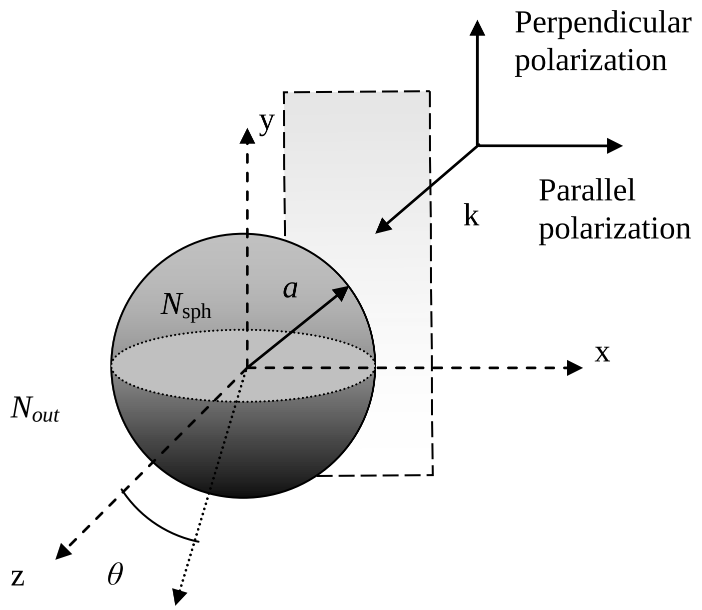

Figure 2.5: Plane-wave excitation geometry for a sphere.

LMT results are shown in figure 2.6 using FORTRAN simulation by S.C. Hill et al. [69].

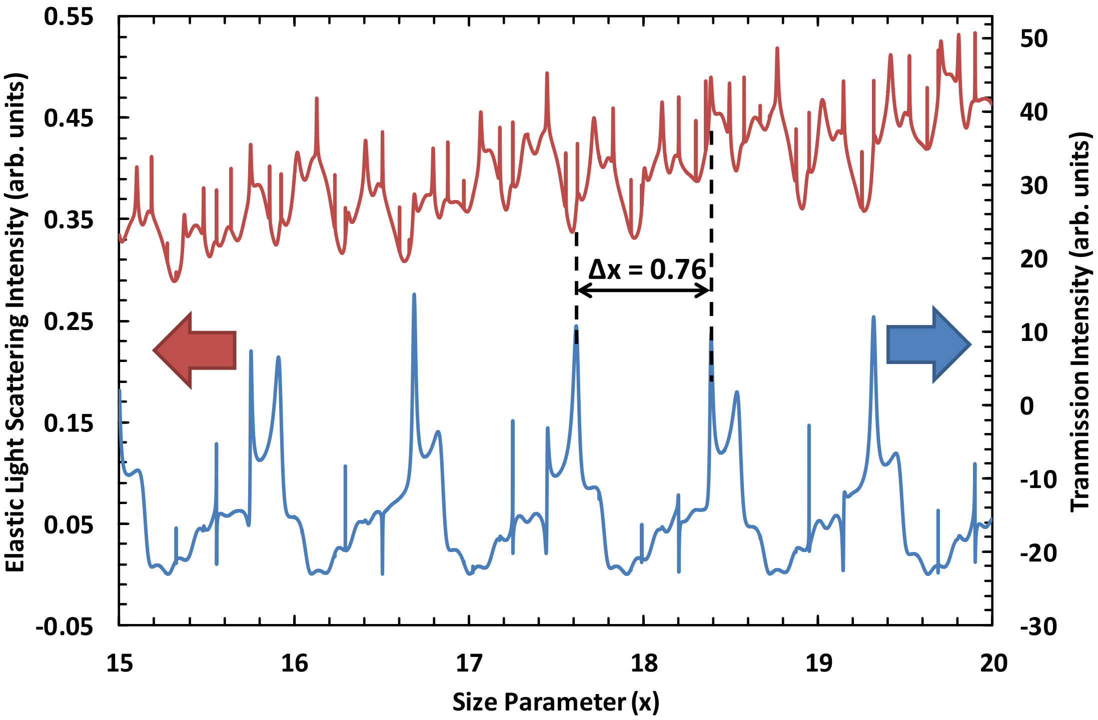

Figure 2.6: LMT simulation for a Si microsphere with x = 15 to 20.

Figure 2.6 shows the elastic light scattering and transmission spectra for a silicon sphere with a size parameter ranging from 15 to 20 for the perpendicular polarization to the plane of incidence. The primary horizontal axis shows the 90° elastic light scattering spectra (in blue) while the secondary horizontal axis shows the 0° transmission spectra (in red). The mode spacing is found using equation 2.6 and it is numerically verified as well in the plot i.e., 0.76 between two consecutive resonant peaks.

2.4.2. Generalized Lorenz-Mie Theory

We know from the previous section that LMT shows us the elastic light scattering results of a spherical body hit by a plane wave. However, when the plane wave is changed in to a focused Gaussian beam then the LMT becomes generalized Lorenz-Mie theory (GLMT).

Therefore the illumination of a spherical body by a Gaussian beam is known as the GLMT, since it is a generalization of the original LMT. In GLMT, the waves having angular mode number smaller than size parameter are excluded from the LMT infinite series [5]. We already know from equation 2.3 and 2.4 that to excite modes of a sphere, the resonance condition must be met. The scattering geometry for GLMT is described in figure 2.7, where ω_o is the half width of the Gaussian beam, *b* the impact parameter, *a* the radius, and N_{sph} is the real part of the sphere's refractive index.

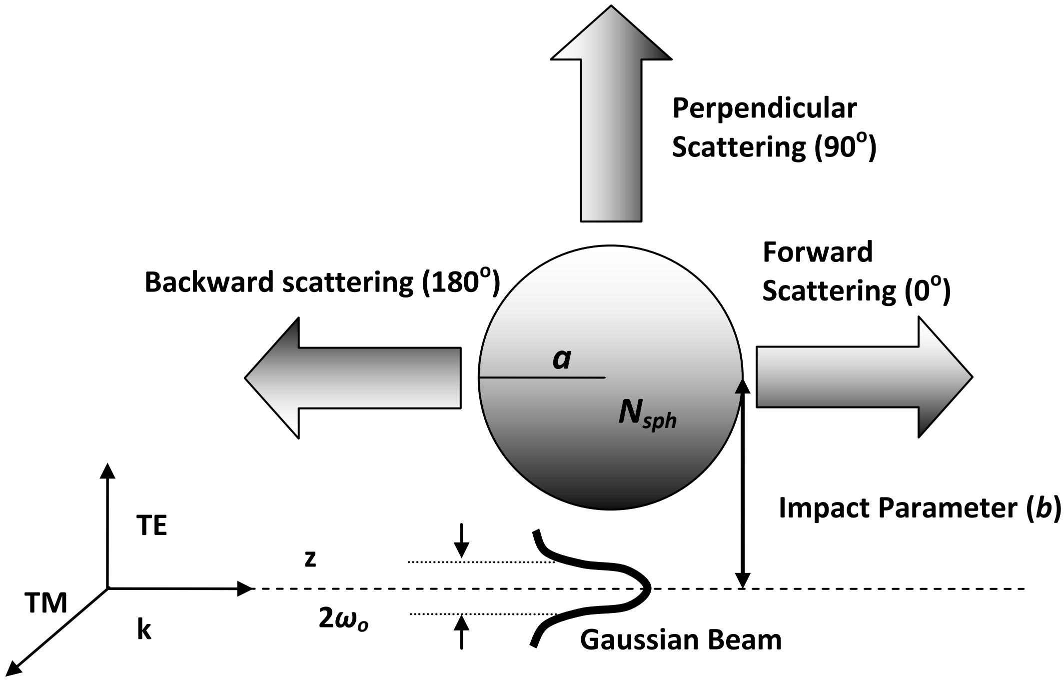

Figure 2.7: Gaussian beam excitation illustration.

Keeping figure 2.7 in mind and by applying the localization principle, the resonance boundaries for the GLMT case are given by rewriting equation 2.4 as:

$$a < b < aM_{sph} \quad (2.8),$$

where *b* is the impact parameter and *a* is the radius of the sphere. The mode spacing for two consecutive peaks as a function of size parameter is described by equation 2.7. However mode-spacing can be expressed as a function of wavelength. Mode-spacing as a function of wavelength is given by the following equation:

$$\Delta\lambda = \frac{\lambda_R{}^2 \arctan\sqrt{M_{sph}{}^2 - 1}}{2\pi a N_{out}\sqrt{M_{sph}{}^2 - 1}} \quad (2.9),$$

where N_{out} is the refractive index of the outside medium and M_{sph} is the relative refractive index of the sphere with respect to the outside medium. The simulations for GLMT are performed by using FORTRAN program by J.A. Lock et al. [70].

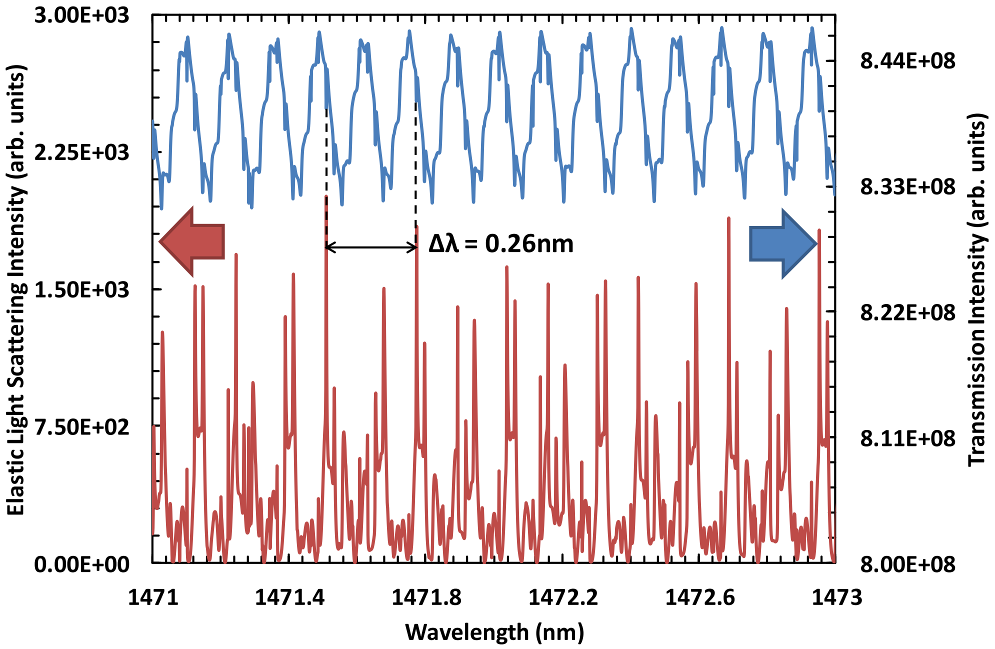

Figure 2.8: TE Polarization scattering spectra of GLMT excitation.

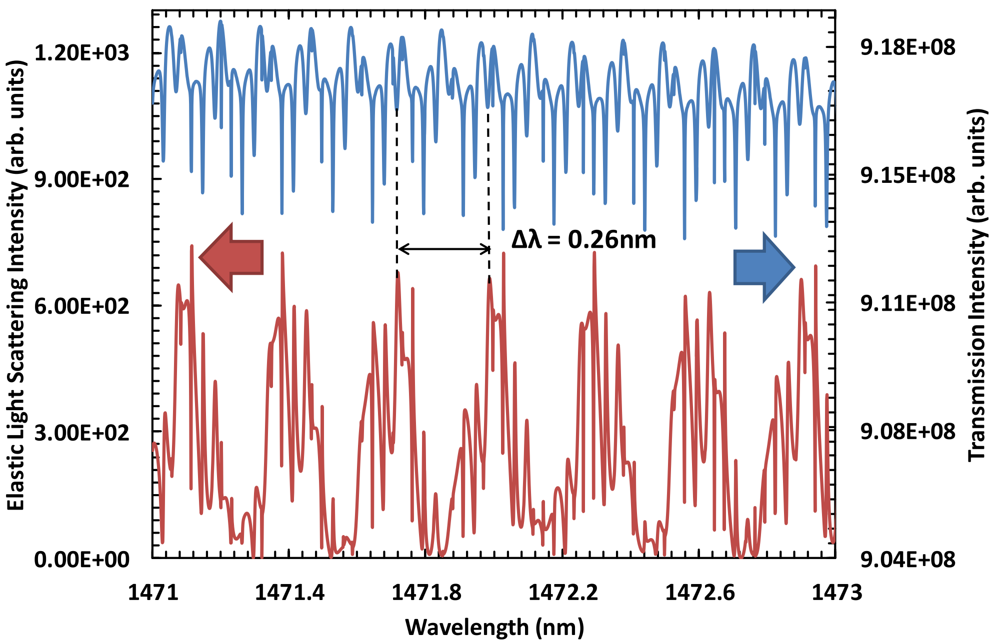

Figure 2.9: TM Polarization scattering spectra of GLMT excitation.

Figures 2.8 and 2.9 show the TE and TM polarization simulation results for GLMT respectively, for a sphere of 500 μm radius, refractive index 3.48, whereas the wavelength range for both scattering spectra plots is from 1471 nm to 1473 nm. The mode spacing for these values was found using equation 2.7 and was found to be 0.26 nm, which agrees with our scattering spectra plots.

2.4.3. Quality Factor of the Resonances

Along with mode spacing the quality factor (Q-factor), is one of the main properties of WGMs. Q-factor is usually defined as the ratio between the energy of the confined photons and the energy of the escaped photons during one circular trip. Q-factor shows the time interval for a photon to stay in the WGM. Therefore, according to the definitions stated above, the Q-factor of the resonances denoted by Q is given by the following equation [71]:

$$Q = \omega\tau \quad (2.10),$$

where, τ stands for the life time of photons and ω stands for the angular frequency. However, Q-factor is also defined as:

$$Q = \frac{\lambda_R}{\lambda_{FWHM}} \quad (2.11).$$

where, λ_R is the resonant wavelength and λ_{FWHM} is linewidth of the resonant peak given by full width at half maximum (FWHM) [72].

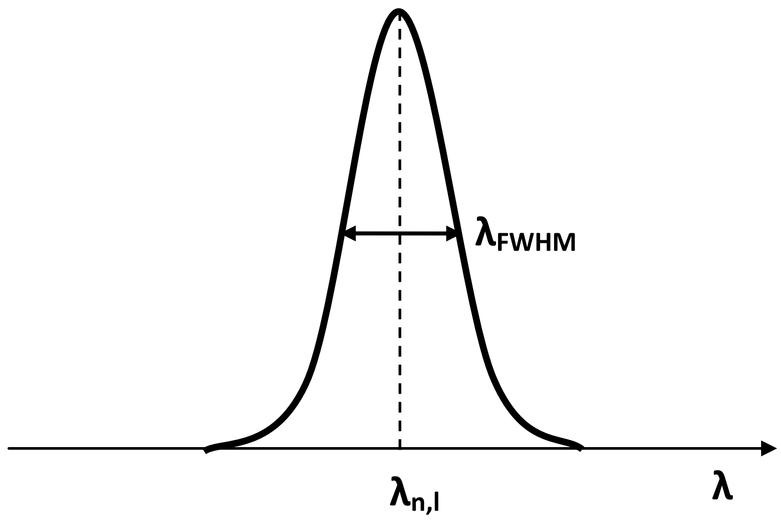

Figure 2.10: FWHM, linewidth of a resonance at a given wavelength.

Figure 2.10 shows the FWHM of a MDR. The angular mode number (*n*) and radial mode number (*l*) directly affect the Q-factor of a MDR. Resonances that are nearer to the surface of the resonator have higher Q-factors [73]. Q-factor is directly proportional to *n*, as *n* increases the Q-factor of the resonator will also increase. The microsphere resonators with a very low radial mode number (*l*) i.e., l=1 and a high polar mode number (*n*), have a high Q-factor.

Chapter 3

OPTICAL EFFECTS IN SILICON

3.1. Silicon Photonics

Solid state microelectronics industry's main material or in other words favorite semiconductor has been silicon for a period of more than half a century [28]. Silicon technology has grown rapidly and Moore's law has continued to hold true for fifty years, and silicon has been an essential component in the growth of the complementary metal oxide semiconductor (CMOS) industry [28], with the main application being in microelectronics [74]. A significant amount of research in silicon photonics has been performed due to the need for high speed communication, cheap photonic devices, high bandwidth, low power and low interference devices in microelectronics [74]. For several applications in microelectronics silicon is one of the mostly used materials and silicon is the basis of many integrated circuits and microprocessors. But there have been several question marks regarding the suitability of silicon in the photonic integrated circuits, however with arrival of the new millennium the tide has turned and semiconductor devices are approaching performance saturation, hence silicon is now seen as a material for manufacturing optoelectronic devices, since silicon photonics is compatible with CMOS technology [29]. Although silicon photonics is relatively a new field, when compared to other semiconductors such as the direct bandgap III-V semiconductor photonics technologies; silicon is enroute to make a huge impact in the field of optical communications [32]. Integrated optoelectronic silicon chips have become the top candidate for succeeding conventional microelectronics [33].

Silicon is highly producible, naturally abundant and a relatively cheap material and is very well researched, and hence is a material well known in electronics [75,76]. Silicon is transparent at the telecommunication wavelengths between 1.3 μm and 1.55 μm, by keeping all these facts in mind silicon photonics is capable to make a great impact in optical communications [77].

3.2. Optical Modulators

One of the main applications of silicon in photonics is being used as the material for a waveguide. Silicon is a suitable material for waveguiding with very low loss. Silicon is transparent from the wavelengths of 1.1 μm extending well into the far-infrared region. We've already seen the theory of a silicon microsphere as a microresonator in chapter 2. However, here we're going to shed some light on the application of silicon waveguides/resonators as optical modulators.

An optical modulator is a device that is used to modulate i.e., change the fundamental properties of a light beam propagating either in free space or in an optical waveguide [40]. An optical modulator can alter different beam parameters, allowing them to be categorized as either, (1) phase modulators, (2) amplitude modulators, and (3) polarization modulators.

Optical modulation is one of the basic requirements for semiconductor microresonators in integrated optics. Optical modulation is usually achieved by altering the optical field of the waveguide/resonator by applying an external signal. The change in optical field actually leads to a change in refractive index. Modulation in silicon is achieved by similar means, i.e., by altering the refractive index. The refractive index of silicon can be changed by three different modulation techniques, such as (1) electro-optic modulation, (2) thermo-optic modulation and (3) all-optic modulation.

3.3. Electro-optic modulation

Electro-optic modulation is achieved in a resonator by applying an electric field to the resonator, electro-optic modulation is further classified into (1) electro-refractive modulation, and (2) electro-absorptive modulation. In electro-refractive modulation, after applying an electric field around the resonator, the real part of the refractive index changes, while in electro-absorptive modulation, the imaginary part of the refractive index changes after application of an electric field around the silicon resonator. The primary effects, that are usually responsible for causing either electro-absorption or electro-refraction in semiconductor materials, are the Pockels effect, the Kerr effect, the Franz–Keldysh effect, while carriers can either be injected or depleted electrically as well.

3.3.1. Pockels effect

Pockels effect is also called the linear electro-optic effect, and is named after a German physicist named Friedrich Carl Alwin Pockels. The Pockels effect is classified as an electro-refractive process, since after the application of an electric field around the material a change in the real part of the refractive index is observed, and is linearly dependent on the applied electric field (E field). The refractive index change will be directly proportional to the applied potential difference, in case of fixed modulator geometry and a uniform constant E field. Moreover, due to Pockels effect a change in the real part of the refractive index is observed, which is dependent on the direction of the E field applied to the modulator, and with respect to the axes of the modulator crystal. Therefore Pockels effect is classified as a polarization dependent process.

Pockels effect requires a lack of inversion symmetry in the material, however since silicon does not possess the lack of inversion symmetry, therefore Pockels effect is non-existent in silicon [75]. The change in refractive index due to Pockels effect is given by the following equation.

$$\Delta N = -\frac{rNE}{2} \qquad (3.1),$$

where ΔN is the change in the refractive index due to Pockels effect, r the linear electro-optic or Pockels coefficient, E the applied electric field and N the refractive index in the direction of the applied E field. Usually the values for r lie in the range 10^{-12} to 10^{-10} m/V for $E = 10^6$ V/m. The change in refractive index due to Pockels effect is very small. Most commonly used crystals to observe Pockels effect are $NH_4H_2PO_4$ (ADP), KH_2PO_4 (KDP), $LiNbO_3$, $LiTaO_3$, and CdTe [78].

3.3.2. Kerr Effect

The Kerr effect is named after a Scottish physicist John Kerr, who discovered the effect in 1875 [79]. Kerr effect is also known as the quadratic electro-optic effect, and results in change in the refractive index proportional to the square of the electric field. Kerr effect is also classified as an electro-refractive process. All materials display the Kerr effect, but it is generally much weaker than the Pockels effect.

In silicon Kerr effect is very weak. Kerr effect is a second order effect and the applied electric field is squared and there is no dependence on the direction of the applied Electric field, unlike Pockels effect. The change in refractive index induced by Kerr effect is given by the following equation:

$$\Delta N = -\frac{sNE^2}{2} \qquad (3.2),$$

where *s* is the Kerr coefficient, E^2 the square of the applied electric field and *N* the initial refractive index. Typical values of G are 10^{-18} to 10^{-14} m^2/V^2 in crystals and 10^{-22} to 10^{-19} m^2/V^2 in liquids [79].

3.3.3. Franz-Keldysh effect

Unlike Pockels and Kerr effect, Franz-Keldysh effect is an electro-absorptive process, since a change in the imaginary part of refractive index of the material is observed after application of an electric field. This effect is named after the German physicist Walter Franz and Russian physicist Leonid Keldysh. The Franz-Keldysh effect is very weak in silicon, while at the telecom wavelengths the Franz-Keldysh effect almost disappears in silicon.

Franz-Keldysh effect is usually strong at wavelengths closer to the bandgap of a semiconductor material. The energy bands of the semiconductor experience a distortion due to the applied voltage, which results in a shift of the energy bandgap. In turn, the energy bandgap shift results in the absorption of the semiconductor. In order to observe a change of the order of 10^{-4} in the refractive index, a potential difference of 200 kV/cm is needed [80]. When compared to Kerr effect, in order to observe a change of the similar in the refractive index, a potential difference of 1000 kV/cm has to be applied.

3.3.4. Electrical carrier injection or depletion

A change in the refractive index of a semiconductor material can also be caused by changing the concentration of free charges. Drude-Lorentz equation for the concentration of free charges to the absorption of the material is:

$$\Delta\alpha = \frac{e^3\lambda_o^2}{4\pi c^3\varepsilon_0 n}\left(\frac{C_e}{\mu_e(m_{ce}^*)^2} + \frac{C_h}{\mu_h(m_{ch}^*)^2}\right) \tag{3.3}$$

where C_e and C_h are concentration of electrons and holes, respectively, α the absorption coefficient, λ_o the vacuum wavelength, c the speed of the light in vacuum, and ε_o the permittivity of the vacuum The corresponding equation for the change in the real part of refractive index is:

$$\Delta N = \frac{-e^2\lambda_0^2}{8\pi^2 c^2\varepsilon_0 n}\left(\frac{C_e}{m_{ce}^*} + \frac{C_h}{m_{ch}^*}\right) \tag{3.4}$$

The relation between the refractive index of silicon and the concentration of hole and electron densities has been studied experimentally by R.A. Soref et al. [80], with special emphasis on the telecommunication wavelengths of 1.3 μm and 1.55 μm. The conclusion for the experimental study was that, the results for silicon are related to Drude-Lorentz model for electrons, whereas, for holes there is a dependence of $(\Delta C_h)^{0.8}$ The following expressions were produced evaluating the changes in the refractive index of silicon due to carrier injection or depletion at communication wavelengths of 1.3 μm and 1.55 μm.

For λ = 1.55 μm.

$$\Delta N = \Delta N_e + \Delta N_h = -[8.8 \times 10^{-22}\, \Delta C_e + 8.5 \times 10^{-18}\, (\Delta C_h)^{0.8}]$$

$$\Delta\alpha = \Delta\alpha_{\mathrm{e}} + \Delta\alpha_{\mathrm{h}} = 8.5 \times 10^{-18}\, \Delta C_e + 6.0 \times 10^{-18}\, \Delta C_h \qquad (3.5),$$

For λ = 1.3 μm:

$$\Delta N = \Delta N_e + \Delta N_h = -[6.2 \times 10^{-22}\, \Delta C_e + 6.0 \times 10^{-18}\, (\Delta C_h)^{0.8}]$$

$$\Delta\alpha = \Delta\alpha_{\mathrm{e}} + \Delta\alpha_{\mathrm{h}} = 6.0 \times 10^{-18}\, \Delta C_e + 4.0 \times 10^{-18}\, \Delta C_h \qquad (3.6),$$

where ΔN_e and ΔN_h are the changes in the refractive index of silicon due to a change in the electron and hole concentrations; whereas $\Delta\alpha_e$ and $\Delta\alpha_h$ are the changes in the absorption coefficient of silicon due to a change in the electron and hole concentrations, respectively.

Career injection and depletion either results in an electro-refractive or electro-absorptive process and a change in the real part or the imaginary part of the refractive index is reported.

3.4. Thermo-optic Modulation

Thermo-optic modulation is the type of modulation where literal heat is applied to the resonator to change its refractive index. Thermo-optic modulation has been demonstrated by installing a heater in the structure such as a waveguide or resonator, which heats the structure and changes its refractive index, thermo-optic modulation has been demonstrated in a silicon Fabry-Pérot etalon [37,38] and a shift in wavelength was observed by heating Nd^{+3} doped silica microspheres [39].

3.4.1 Thermo-optic coefficient of Silicon

The thermo-optic coefficient of silicon is given by the following equation:

$$\frac{\Delta N}{\Delta T} = 1.86x10^{-4} / K \qquad (3.7),$$

where ΔN is the change in the refractive index of silicon and ΔT is the change in the temperature of silicon. The thermo-optic coefficient of silicon is considerably higher than that of silica and other thermo-optical materials.

3.5. All-optical Modulation

All-optical control, such as modulation, and switching, is usually achieved by using a light source to control another light source. A pump laser is used to control the resonances of a probe laser, which is used for excitation. All-optical modulation is usually either attributed to the two photon absorption (TPA), or to the linear one photon absorption (OPA).

3.5.1. One/Two-Photon absorption

One photon absorption (OPA) is a linear process and is also called linear absorption, whereas the two photon absorption (TPA), is a non-linear process. OPA or TPA are induced by using a focused pump beam or a coupled pump beam. In OPA one photon is absorbed, whereas in TPA, two photons are simultaneously absorbed, which results in the excitation of the carrier to high energy level, for example from the valence band to the conduction band [81]. TPA depends on the optical absorption. If the combined energy of the single or the two incident photons is greater than the bandgap energy of silicon ($E_g = 1.12$ eV, $\lambda = 1100$ nm), then they will be absorbed and will excite an electron from valence band to conduction band, which will in turn result in the generation of heat in the form of a phonon, when the electron transitions in the conduction band, i.e., intraband transition, and interband transition will result in the emission of photon. In silicon, TPA occurs at high intensity of the pump laser, since it is a non-linear process, whereas OPA occurs at lower intensity.

3.5.2. Free carrier absorption and dispersion

Both OPA and TPA lead to free carrier absorption (FCA) and free carrier dispersion (FCD). Since, we have already discussed the generation of phonon above, if the free carrier lifetime is small, it will take little time to recombine and therefore will result in generation of heat i.e., phonons which in turn results in the thermo-optic effect (TOE). Free carrier absorption (FCA) and free carrier dispersion (FCD) are the all-optical counterparts of electro-absorption and electro-refraction, respectively. In FCA a change in the imaginary part of the refractive index is observed and, in FCD a change in the real part of the refractive index is observed. FCA in turn results in the TOE, which causes a redshift in the resonances of the silicon microresonator. FCD results in blueshift and depends on the free carrier lifetime. FCA is usually the dominant process in silicon microresonators, but if the free carrier lifetime is increased in the silicon microresonators, it will result in FCD being the dominant process and a blueshift in the resonances will be observed. FCD and FCA are explained, using the Drude-Lorentz model already give in equations 3.5 and 3.6.

3.5.3. Thermo-optic effect induced by free carrier absorption

OPA and TPA are induced by using a focused pump beam or a coupled pump beam lead to free carrier absorption (FCA) and free carrier dispersion (FCD), which are the all-optical counterparts of electro-absorption and electro-refraction, respectively. FCA results in thermo-optic effect (TOE) and generation of heat in the form of phonons and due to the high thermo-optic coefficient of silicon. Whereas TOE results in red-shift of the spectrum and FCD results in blue-shift of the spectrum. Due to the high thermo-optic coefficient of silicon red-shift is observed, after using OPA to induce TOE. FCD can be made the dominant process by increasing the free carrier lifetime. The TOE in silicon is strong at low frequencies, therefore TOE overshadows the rest of the nonlinear effects at millisecond regime. The chief advantage of the thermo-optic based switching is that it is not dependent on the polarization switching speeds [82].

All-optical modulation has been demonstrated in different types of resonators such as silicon and silicon nitride microrings. Similarly wavelength shifts have been observed for microspheres of different materials such as silica, silica coated by silicon, and chalcogenides. However, here for the very first time to our knowledge, we report all-optical switching in silicon microspheres in the near-Infrared by Thermo-optic effect (TOE) induced by one photon absorption (OPA).

Chapter 4

ALL-OPTICAL RESONANCE TUNING WITH SILICON MICROSPHERE

In this chapter, we will discuss the essence of our work by keeping in mind the optical processes explained in chapter 3. All-optical control such as modulation or switching has been demonstrated several times in silicon microresonators, however we demonstrate it for the first time in silicon microspheres. As already explained that all-optical control requires a pump light source and a probe light source to achieve all-optical control, therefore we go step by step in the chapter by first analyzing the probe laser and then the pump laser.

4.1. Elastic Scattering Spectra of the Probe laser

The experimental setup used for exciting the WGMs in the silicon microsphere illustrated in figure 4.1. A single silicon microsphere of 1 mm diameter and refractive index 3.48 is placed on a silica optical fiber half b coupler (OFHC) manufactured from a single mode optical fiber. The OFHC is connected to a near-IR distributed feedback (DFB) laser with the central wavelength of 1472 nm, to excite the WGMs of the microsphere. The DFB laser is controlled using a laser diode controller (LDC). A photodiode is placed over the eyepiece of the microscope to collect the elastically scattering data. One end of the OFHC is connected to the DFB laser while the second end is connected to another InGaAs photodiode for the purpose ,of collecting the transmission data.. The outputs from the two InGaAs photodiodes, silicon photodiode, and the signal generator are connected to a digital storage oscilloscope (DSO), while the DSO is connected to a computer, where the data is recorded using Labview software.

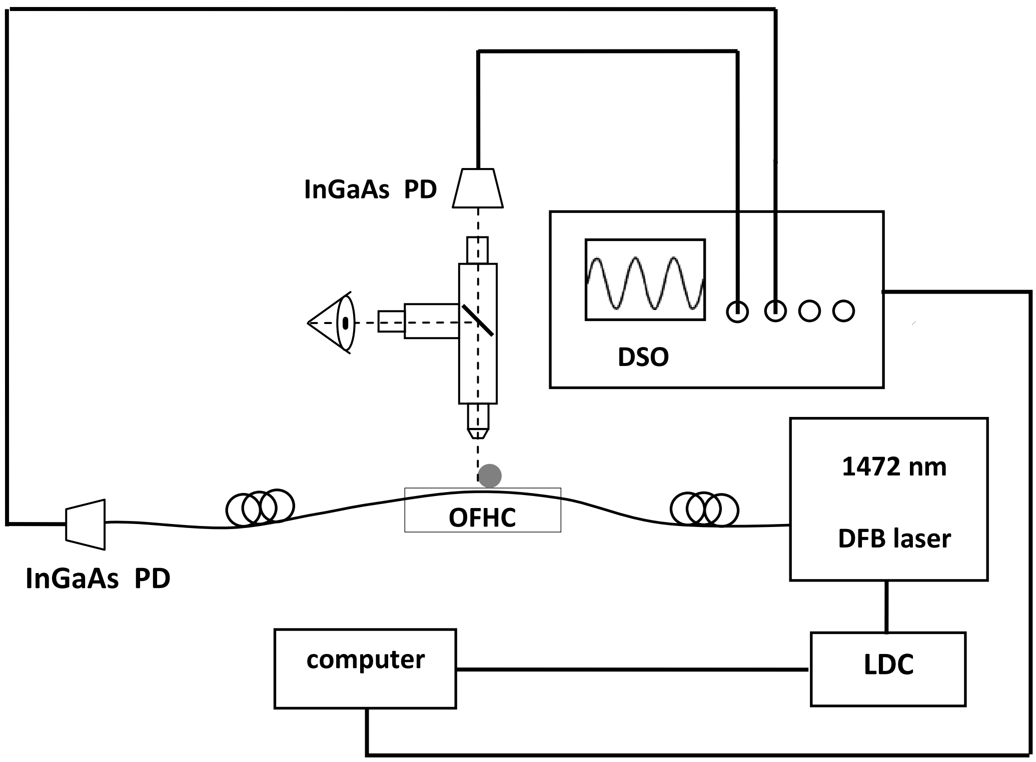

Figure 4.1: Experimental setup for exciting the WGMs of the silicon microsphere.

Figure 4.2 shows the elastic light scattering results obtained by utilizing the optical setup explained in figure 4.1. A mode spacing of 0.26 nm , and a quality factor of $4x10^4$, is observed using this setup, and there is a visible correlation between the peaks and dips of the transmission and scattering, which agrees with the LMT and

GLMT calculation performed in chapter 2. Hence, our probe laser is functional and giving us the desired results.

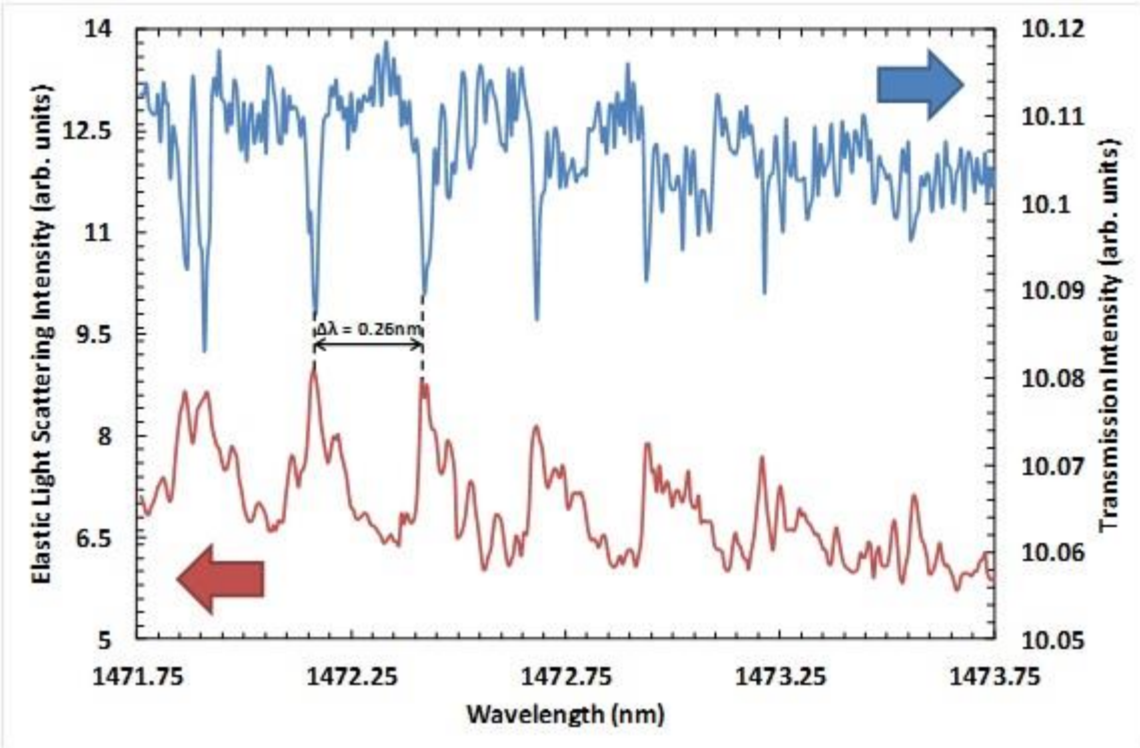

Figure 4.2: Scattering and transmission spectrum of the silicon microsphere.

4.2. Characterization of the Pump using TTL input

After checking the probe laser, now we characterize the pump laser, before performing the all-optical wavelength shift experiment. A TTL input of 0-5V, with 8 Hz frequency (125 ms) is fed to the pump laser to analyze the behavior of the pulses of the electronic function generator and the pump laser. The experimental setup for the characterization process is illustrated in figure 4.3. The output from the electronic function generator is split, where one end is fed to the DSO and the second is fed to the 405 nm Fabry-Pérot pump laser. The output of the pump laser is collected by a silicon photodiode and the output of the silicon photodiode is connected to the DSO. The DSO is connected to a computer, where the data is collected using Labview software.

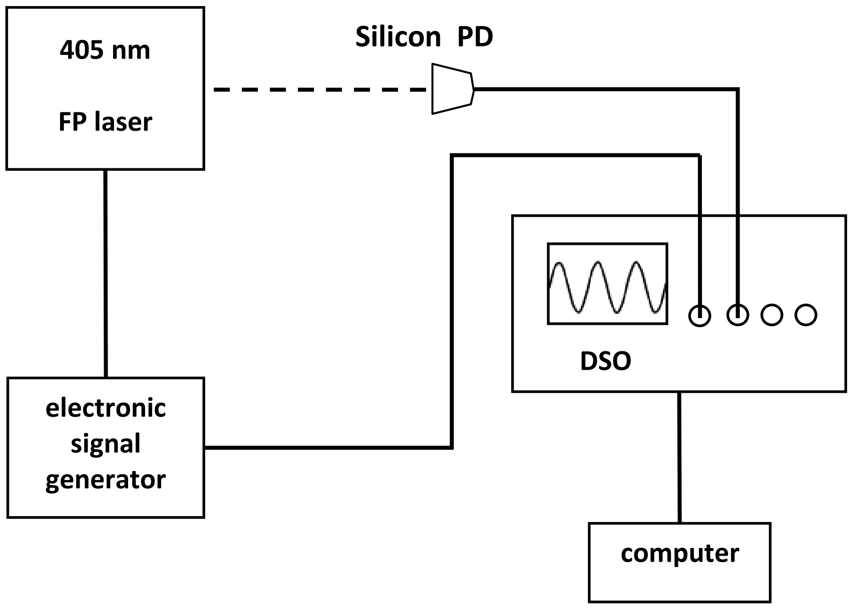

Figure 4.3: Experimental setup for exciting the pump characterization.

Figure 4.4 shows the input signals from the electronic function generator at duty cycles of 20%, 30%, 40% and 50%, while figure 4.6 shows the input signals at the duty cycles of 60%, 70% and 80%. Figures 4.5 and 4.7 show the outputs of the pump laser for the duty cycles of 20%, 30%, 40%, 50% and 60%, 70%, 80%, respectively.

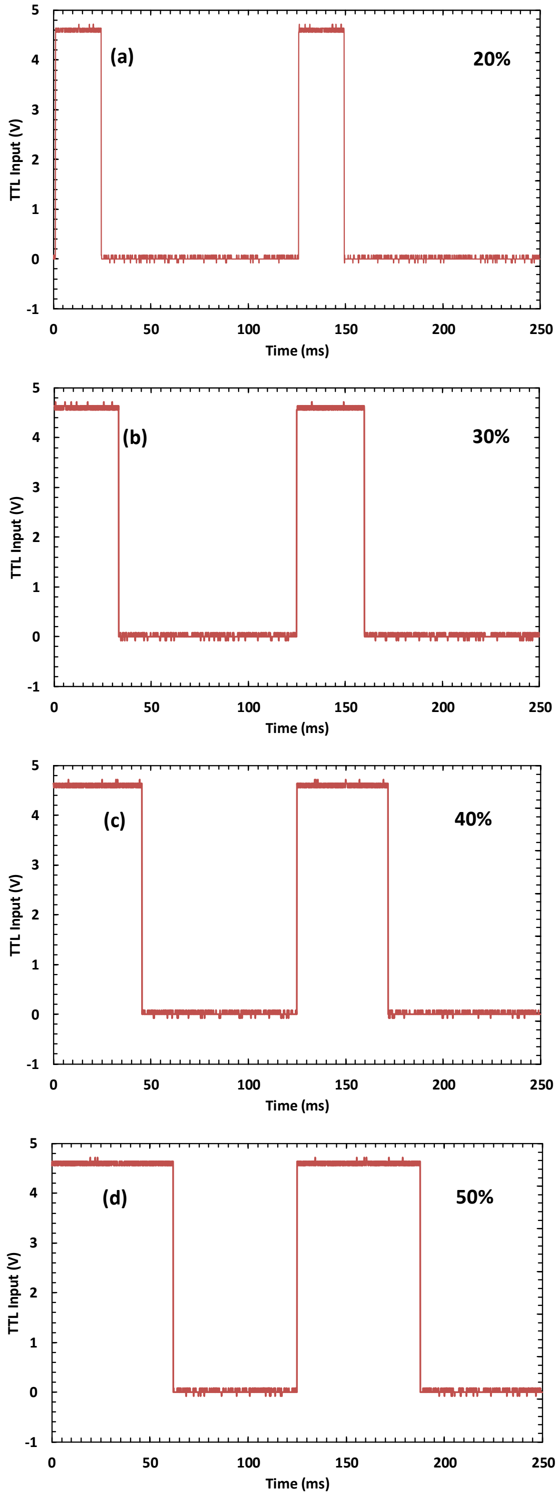

Figure 4.4: Applied signal from at (a) 20% (b) 30% (c) 40% (d) 50% duty cycles.

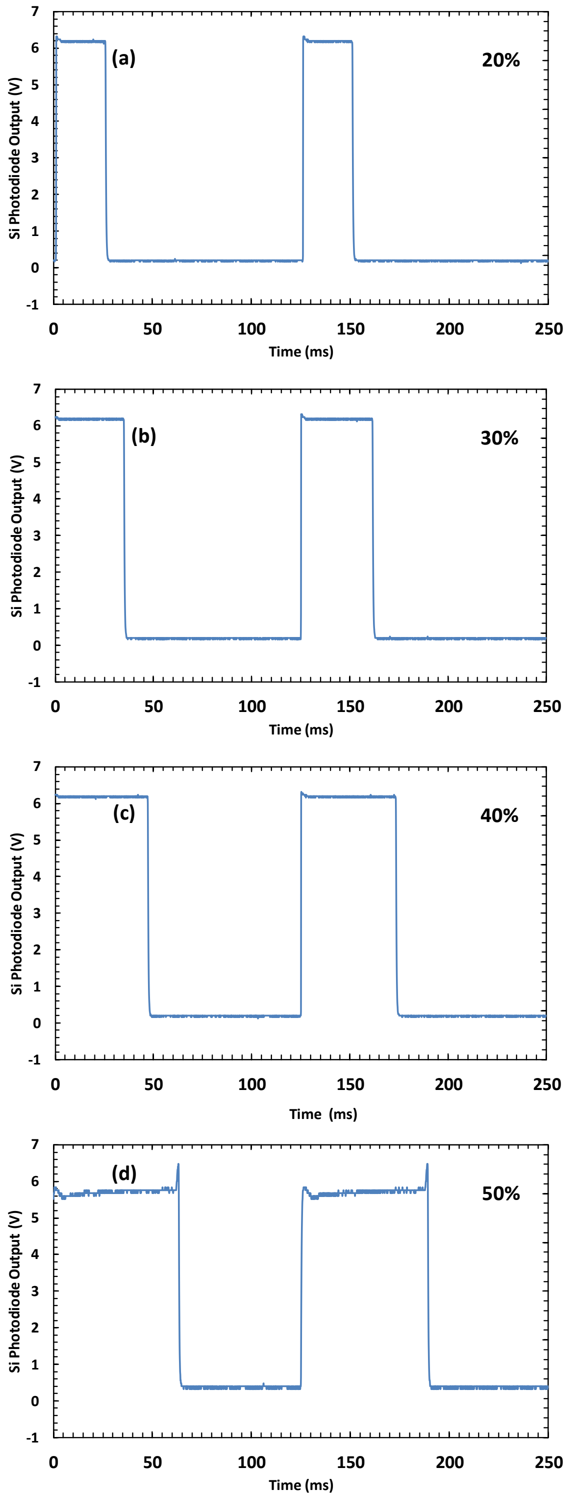

Figure 4.5: Pump laser monitor at (a) 20% (b) 30% (c) 40% (d) 50% cycles.

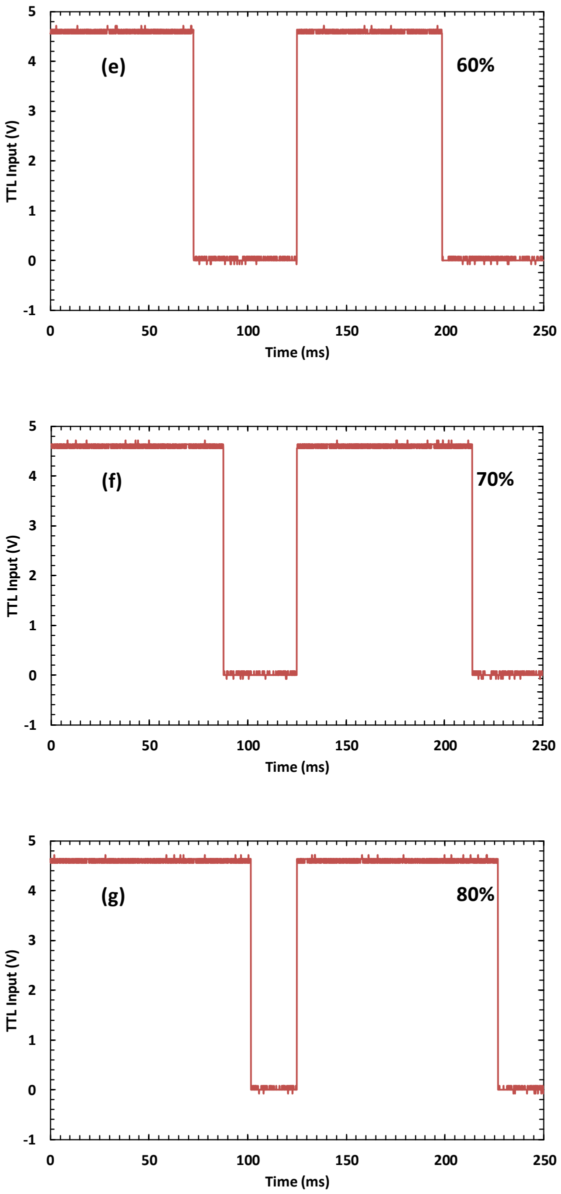

Figure 4.6: Applied signal from EFG at (e) 60% (f) 70% (g) 80% duty cycles.

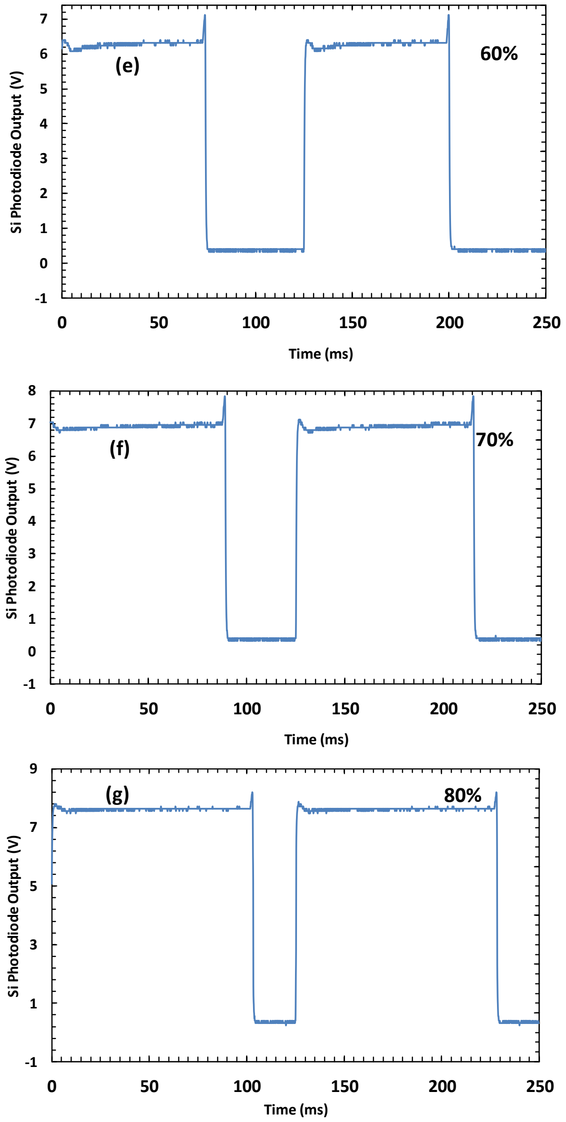

Figure 4.7: Pump laser monitor at (e) 60% (f) 70% (g) 80% duty cycles.

As seen in figures 4.4 and 4.6 the inputs from the electronic function generator are stable and are generating a good pulsed output of 0-5V, similarly good pulsed outputs are observed at the silicon photodiode at a time range of 250 ms in figures 4.5 and 4.7.

	Voltage at Electronic Function generator (V)		Voltage at Silicon Photodiode (V)	
Duty Cycle	Minimum	Maximum	Minimum	Maximum
20%	0	4.64	0	6.28
30%	0	4.64	0	6.32
40%	0	4.64	0	6.28
50%	0	4.64	0	6.4
60%	0	4.64	0	6.96
70%	0	4.64	0	7.76
80%	0	4.64	0	8.12

Table 4.1: Function generator input and, pump laser output comparison.

Table 4.1 shows the comparison between the input from the electronic function generator and the output of the pump laser collected at the silicon photodiode, the output of the function generator remains stable throughout the application of different duty cycles, i.e., 0-4.6 V, however the output of the pump laser changes with the application of the different duty cycles. The output of the pump laser continues to increase with the increase of the duty cycle, due to the increased on time.

4.3. All-Optical wavelength tuning of the Si Microsphere Resonance

The main experimental setup used for this work is illustrated in figure 4.8. After the checking of the pump laser and characterization of the probe laser, both the setups from figures 4.1 and 4.3 are combined to achieve our aim of all-optical control. A single silicon microsphere of 1 mm diameter and refractive index 3.48 is placed on the silica OFHC, manufactured from a single mode optical fiber. The OFHC is connected to a near-IR DFB laser with the central wavelength of 1472 nm, to excite the WGMs of the microsphere. The DFB laser is controlled using a LDC. A photodiode is placed over the eyepiece of the microscope to collect the elastically scattering data. One end of the OFHC is connected to the DFB laser, while the second end is connected to another InGaAs photodiode for the purpose of collecting the transmission data. A pump laser with wavelength of 405 nm is used to control the WGMs excited in the silicon microsphere by the 1472 nm DFB probe laser. The output of the 405 nm pump laser is split using a beam splitter, where one of the split beams is collected by a silicon photodiode, and the other one is focused on the silicon microsphere using convex lens with a focal length of 20 cm. The pump 405 nm laser with an average power of 6.32 mW at 90% duty cycle is focused down to a spot of 170 μm in diameter, corresponding to an average intensity of 28 W/cm^2. The 405 nm pump laser is driven by an electronic signal generator operating at duty cycles of 10% to 90%. A silicon wafer is placed before the objective of the microscope to prevent the InGaAs photodiode from detecting any 405 nm light. The outputs from the two InGaAs photodiodes, silicon photodiode, and the signal generator are connected to a DSO. The DSO is connected to a computer, where the data acquisition and storage is performed using Labview software.

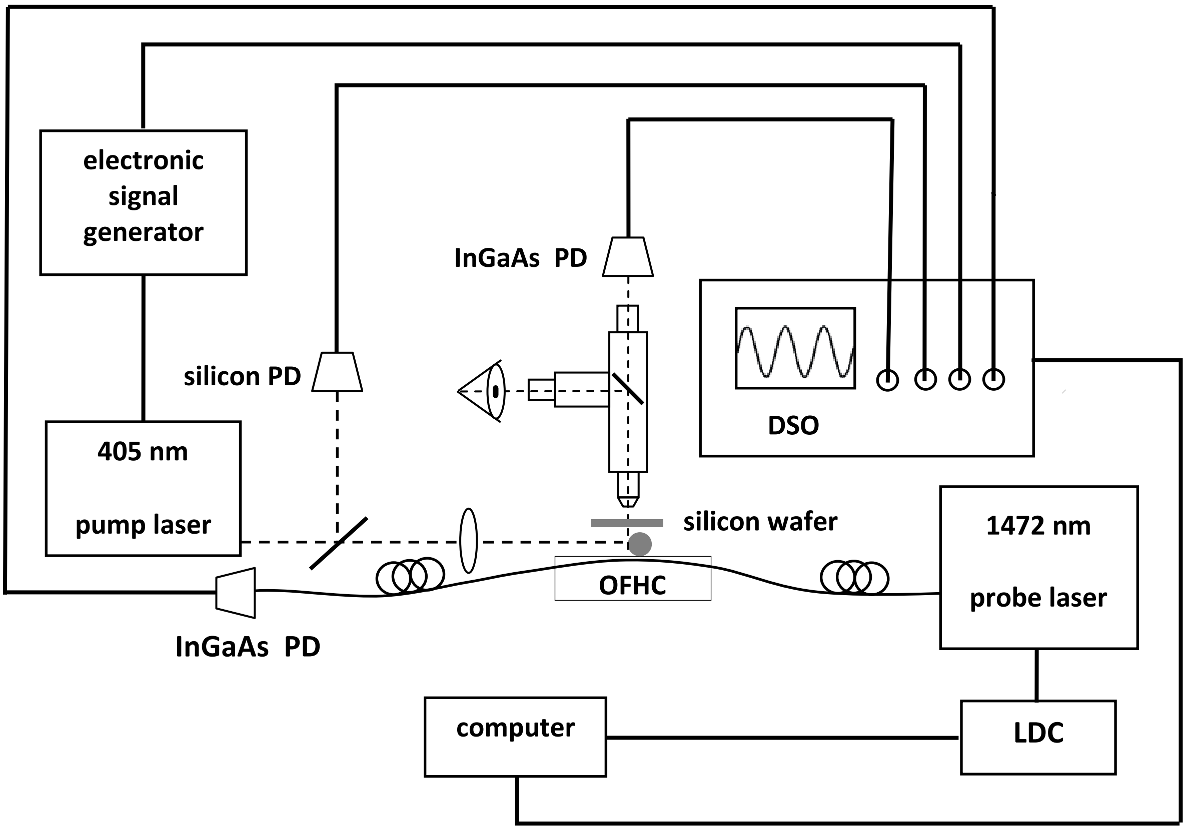

Figure 4.8: Experimental setup of all-optical switching in a silicon microsphere.

4.3.1. Silicon microsphere wavelength tuning with different pump duty cycles

Figure 4.9 (a) and (b) shows the transmission and scattering spectra, when the 405 nm pump laser is operated at 7 Hz with 0% and 20% duty cycle pump signals, respectively. A shift of Δλ = 0.16 nm can be observed, corresponding to an average intensity of 6 W/cm^2 for 20% duty cycle. The change in refractive index is calculated using:

$$\frac{\delta\lambda}{\lambda} = \frac{\Delta N}{N} \quad (4.1),$$

where ΔN is the change in refractive index, N the refractive index of silicon, and $\delta\lambda$ the wavelength shift. For a shift of $\delta\lambda$ = 0.17 nm, the refractive index change was found to be $\Delta N = 4.02 \times 10^{-4}$, while the change in temperature was found to be approximately ΔT = 2K. The red shift in the spectra is attributed to the FCA induced TOE. Similarly, Fig. 4.10 and 4.11, show all the transmission and scattering data with duty cycles of 0%, 20%, 30%, 40%, 50%, 60%, 70%, and 80% and the red shift with the increase of pump laser duty cycle. The average wavelength shift is found to be 0.37 nm for 50% duty cycle, which leads to an average refractive index change $\Delta N = 8.75 \times 10^{-4}$ and an average temperature change ΔT = 4.70 K

Duty Cycle	Change In wavelength	Change in Refractive index	Change in Temperature
-	$\delta\lambda$	ΔN	ΔT
20 %	0.17 nm	4.02×10^{-4}	2.16 K
30 %	0.25 nm	5.91×10^{-4}	3.18 K
40 %	0.31 nm	7.33×10^{-4}	3.94 K
50 %	0.37 nm	8.75×10^{-4}	4.70 K
60 %	0.51 nm	12.06×10^{-4}	6.49 K
70 %	0.58 nm	13.71×10^{-4}	7.37 K
80 %	0.63 nm	14.89×10^{-4}	8.00 K

Table 4.2: Parameter change for the spectra in Figs. 4.10 and 4.11.

Table 4.2 shows the wavelength shift, refractive index change, and the temperature change due to the application of different duty cycles of the pump laser. The change in temperature is calculated using the thermo-optic coefficient equation.

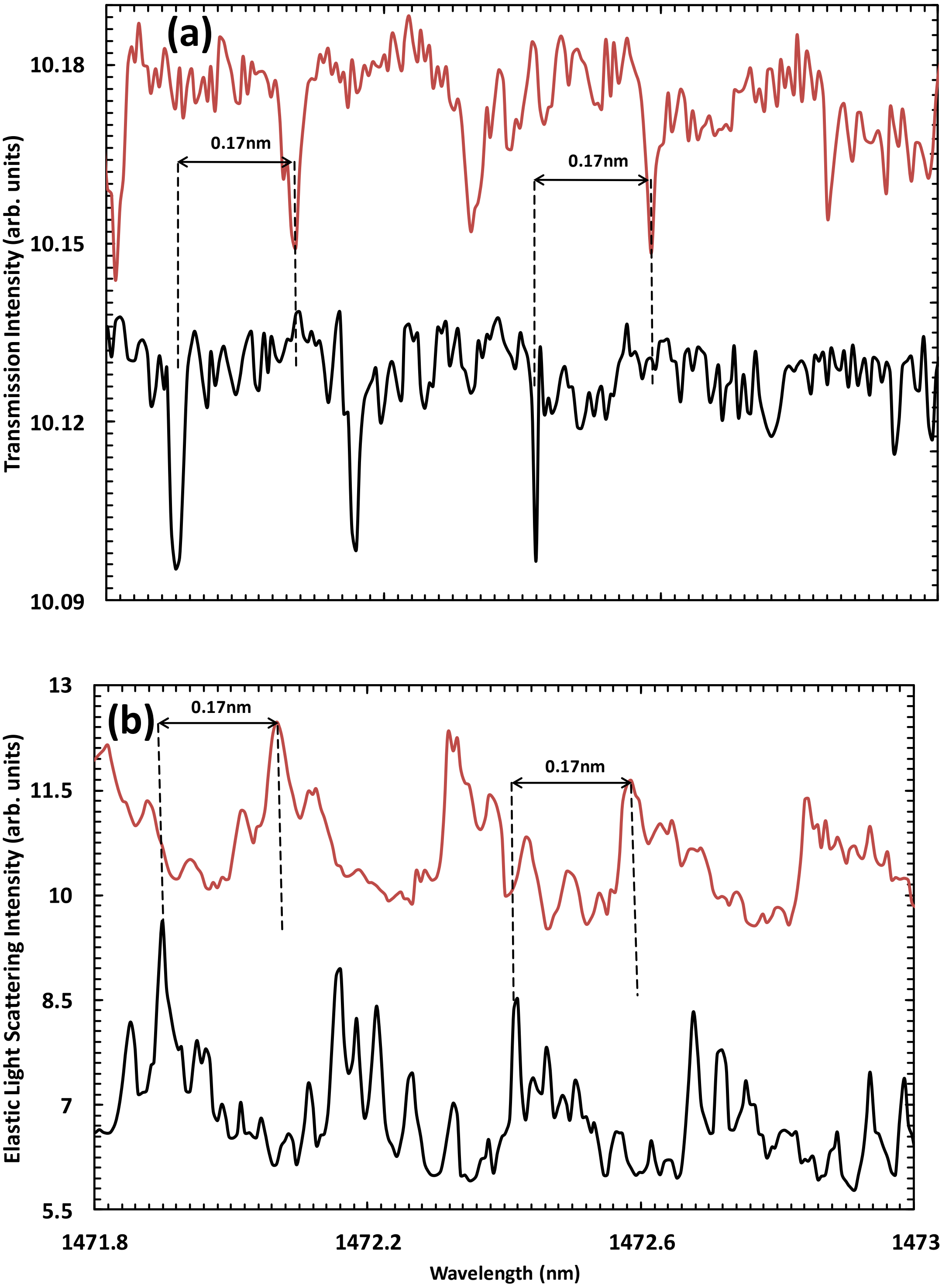

Figure 4.9: Shift in (a) transmission, (b) scattering at 20% duty cycle pump.

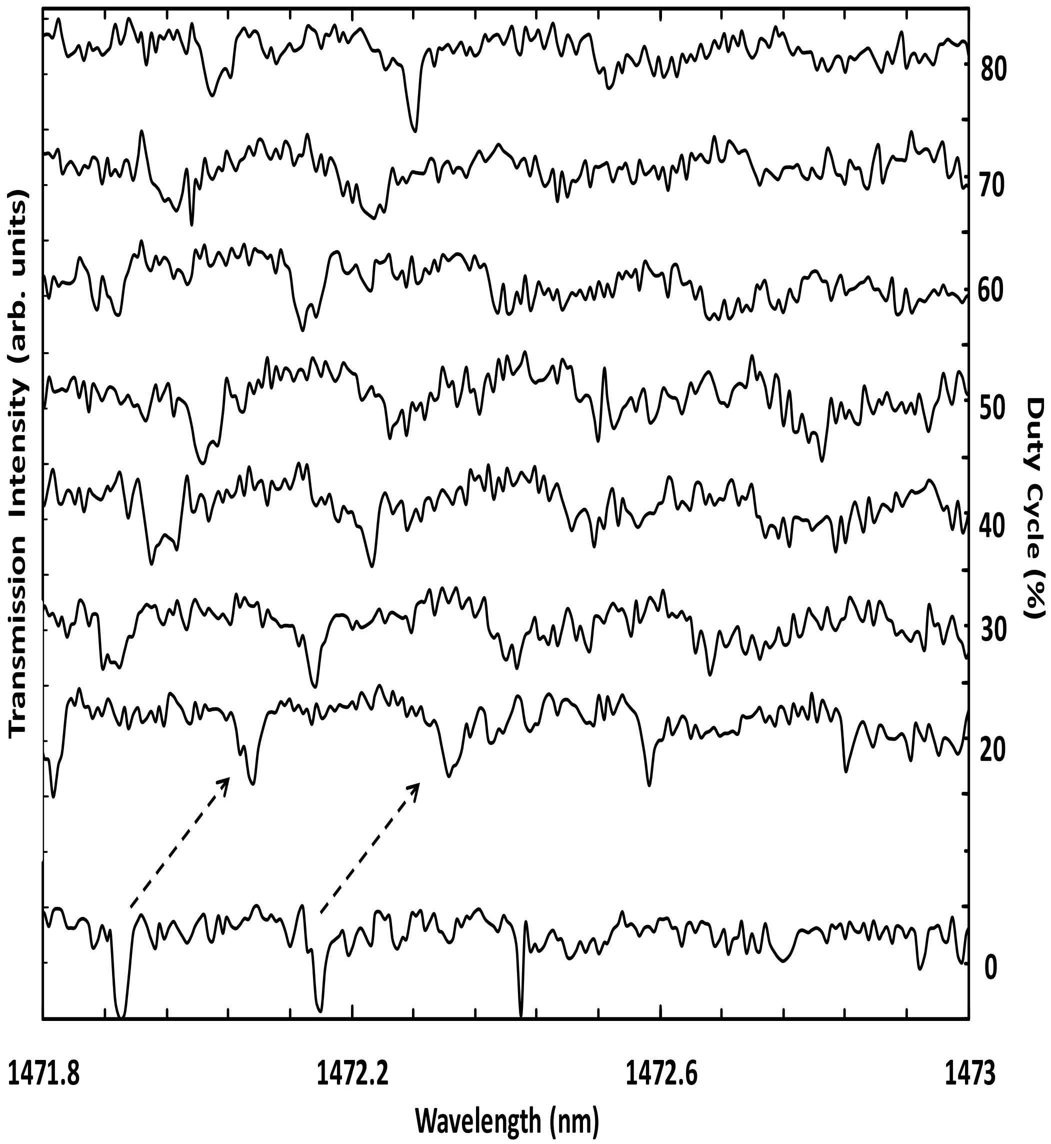

Figure 4.10: Transmission spectra from 0% to 80% duty cycle pump laser.

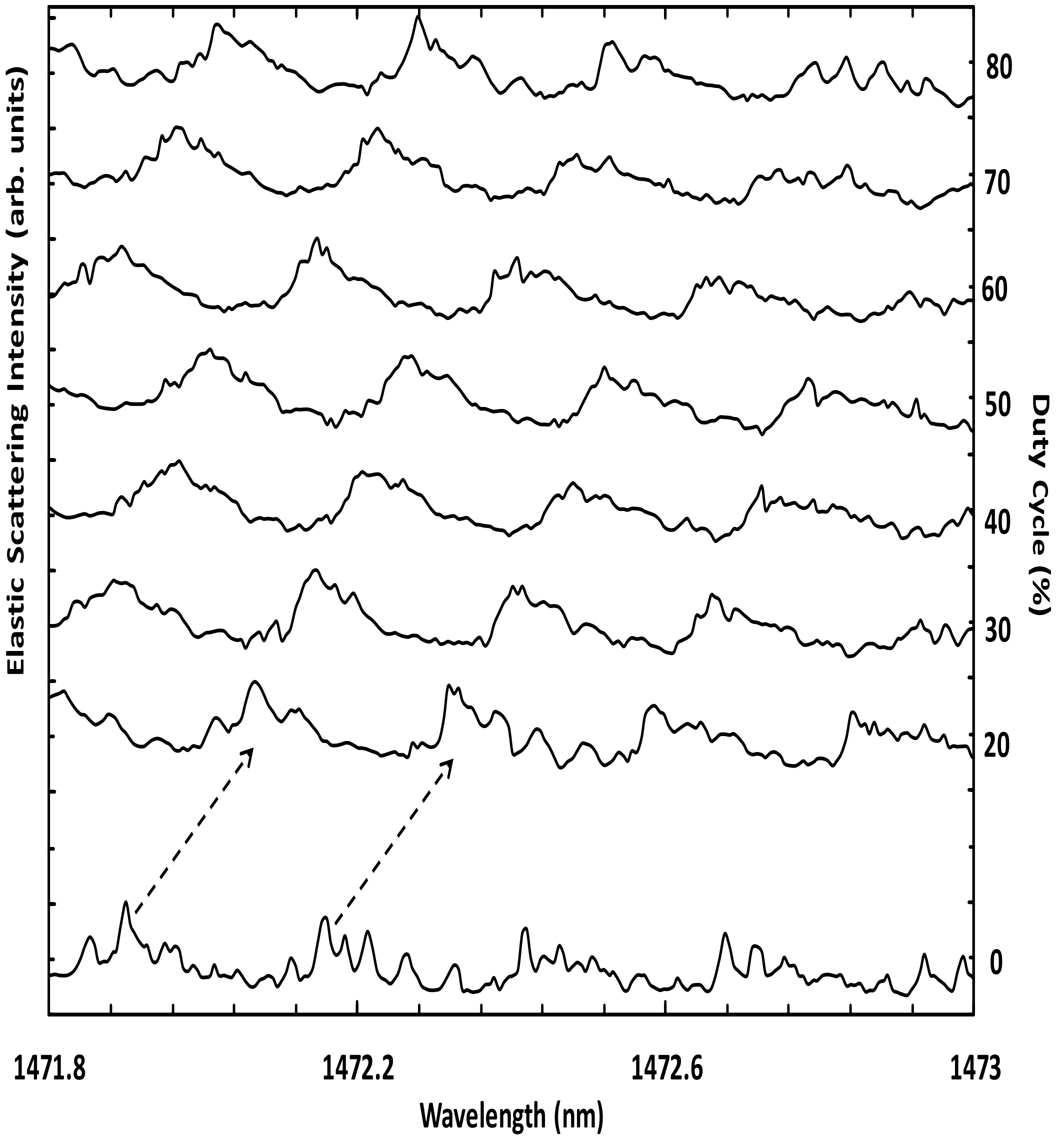

Figure 4.11: Scattering spectra from 0% to 80% duty cycle pump laser

Chapter 5

ALL-OPTICAL SWITCHING IN SILICON MICROSPHERES

In this chapter, the all-optical study of the resonances observed in the previous chapter is performed in time. The experimental setup is kept the same as in figure 4.8, but however the Labview VI (virtual instrument) or in other words the data acquisition software is changed to observe the elastic light scattering signal of the 90^{o} scattering in time. Unlike the study performed in the previous chapter, instead of scanning for a wavelength range, which is usually performed by specifying a temperature range on the LDC, the temperature of the DFB laser is kept at a single temperature near to a resonant peak of elastic light scattering spectra. The equation linking the temperature to wavelength for the probe DFB laser is given by the following equation:

$$\lambda = (0.3587 \times T) + 1467.1 \qquad (5.1),$$

where T is the temperature that the probe DFB laser is operating at.

5.1. Unfocused all-optical switching (AOS) spectra

For this part of the experiment the focusing lens is taken out of the experimental setup to observe the behavior of the elastic scattering single for an unfocused pump laser illuminating the sphere. First an elastic scattering spectra is taken, for temperature ranging from 13 ºC to 20 ºC, which corresponds to a wavelength range of 1471.75 nm to 1474.30 nm. The elastic scattering spectra is shown in figure 5.1.

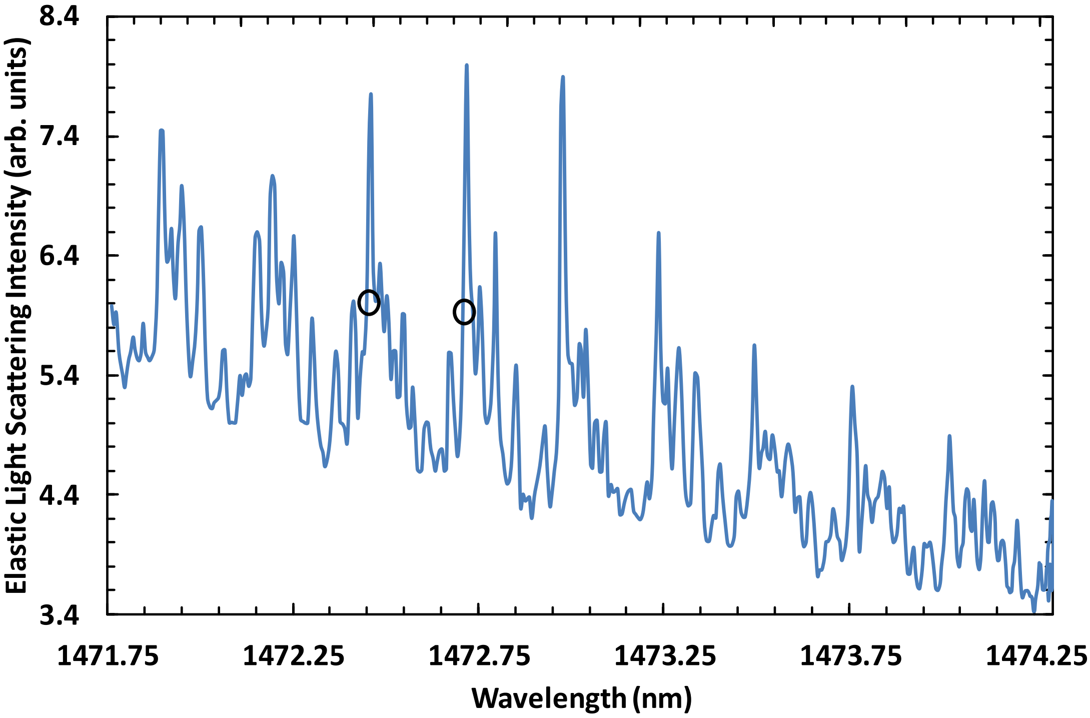

Figure 5.1: Elastic scattering spectrum.

Figures 5.2 and 5.3 show the timing plots of the switched transmission and scattering for various values of the pump duty cycles ranging from 20% to 80% with an increment of 10% steps. For figure 5.2 the temperature at the LDC is fixed at 14.9 ºC and for figure 5.3 the temperature is fixed at 15.6 ºC, which correspond to the wavelengths of 1472.45 nm and 1472.70 nm respectively, that lie at almost one mode spacing apart and are denoted in figure 5.1 via the two circles. The shoulder wavelength values of the resonances are chosen because of the fast rate of change of the slope. In figures 5.2 and 5.3, the 405 nm pump laser is operating at 8 Hz, and all the plots have a time range from 0 to 250 ms, where one grey plus one white portion equal 125 ms, which corresponds well with the applied frequency. The grey portions of the figures show the on time of the duty cycle, whereas the white portions show the off times of the duty cycles of the applied pump signal. It is evident from the figures that during, the on-period of the pulse, a change in the refractive index of silicon is observed, whereas during the off-period the refractive index of silicon goes back to its original value. However, the pattern is not the same throughout the figure, as different duty cycle pump is shone on the microsphere. In some instances, since the duty cycle value is high, the refractive index of the microsphere might not revert back to its original value as quickly as it happens for smaller duty cycle values. However, one thing is clear that, there are patterns in the on-time and off-time duty cycles, which repeat themselves throughout the timing; the effect for the on-time and off-time are opposite of each other, as in some cases the signal goes up in the on time of the duty cycle and it comes down in the same plot for the off time of the duty cycle, which is due to the effect of previously applied duty cycle.

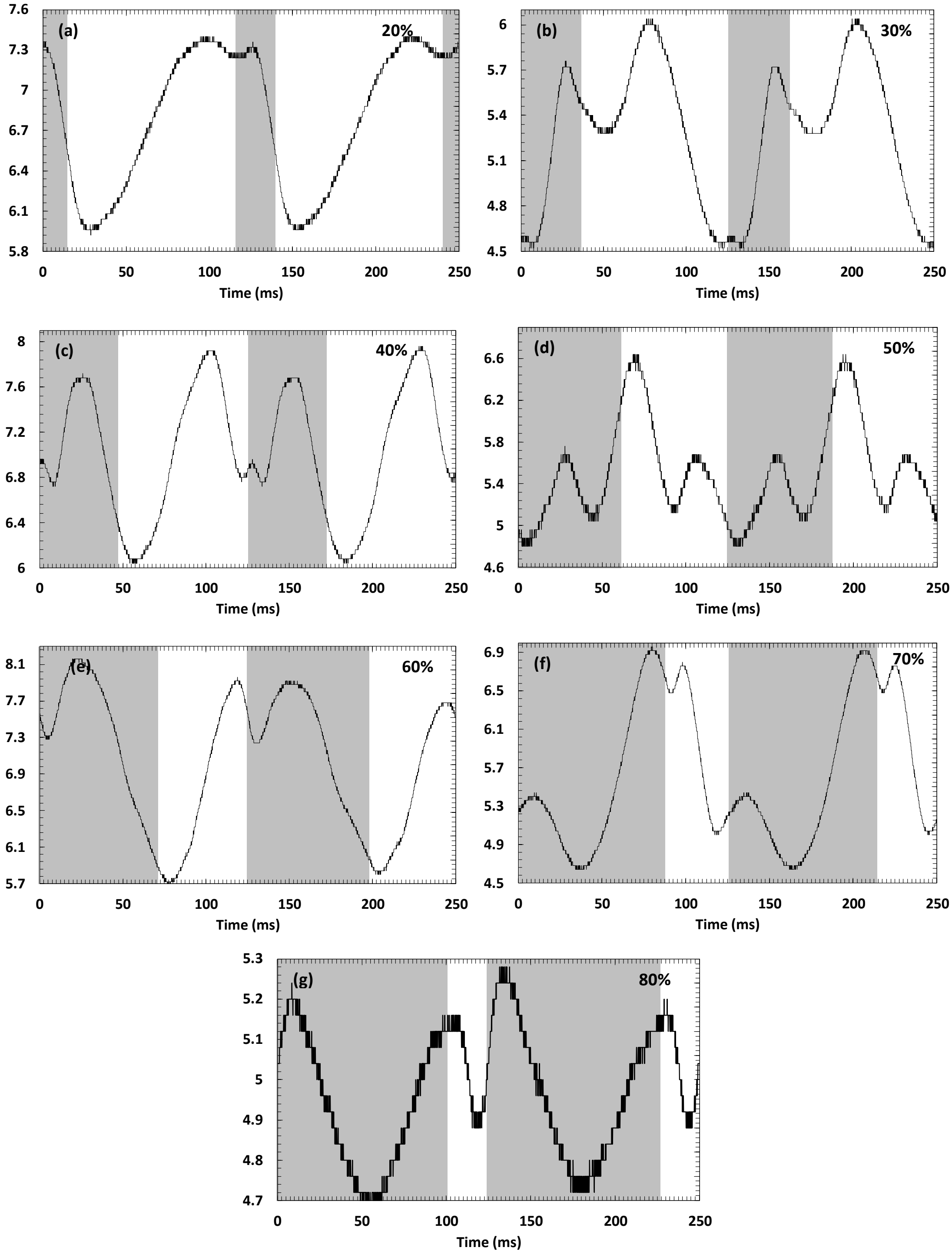

Figure 5.2: Unfocused AOS signal at 8 Hz pump for a 14.9 ºC WGM shoulder.

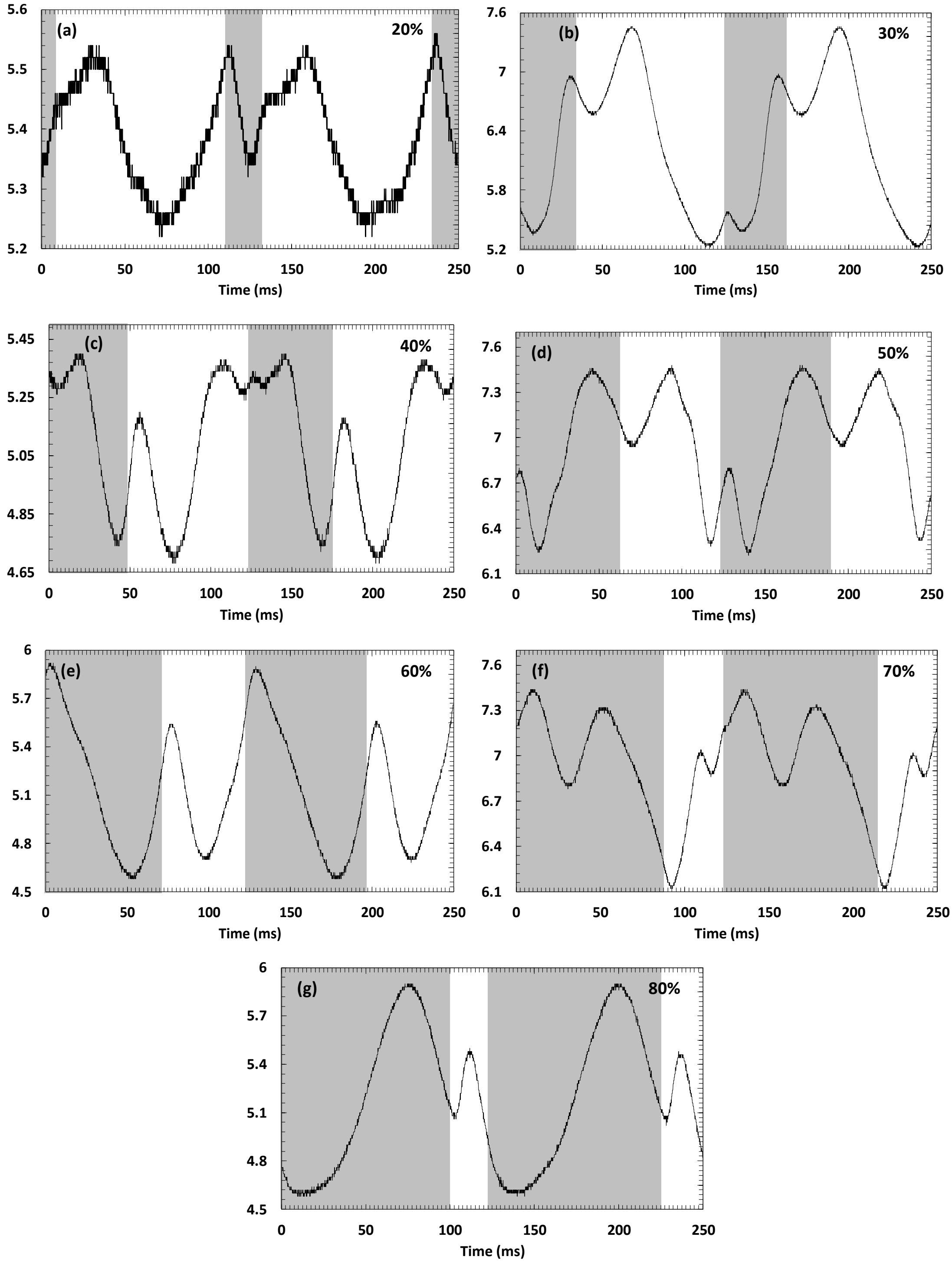

Figure 5.3: Unfocused AOS signal at 8 Hz pump for a 15.6ºC WGM shoulder.

5.2. Off-resonance switching spectra

Another experiment was conducted to verify the claim made in the previous section. This time the sphere was placed at weak coupling spot on the OFHC and an off-resonant spectrum was taken, later on the laser was fixed at a random temperature of 14.9 ºC, to observe the elastic light scattering signal. The frequency was kept the same i.e., 8 Hz and the same pattern of pump duty cycles was followed. The scattering signal spectra are plotted in Figure 5.4 using the same format as Figures 5.2 and 5.3. Apart from Figures 5.4 (b) and (c), no visible repetitive pattern can be found in the scattering signal spectra. This observation shows that the pump laser was used to modify the WGMs of the silicon microsphere induced by the probe laser, which are evident in Figures 5.2 and 5.3. Since no repetitive pattern can be seen in the spectra, therefore it is shown that the elastic scattering signal pattern observed was due to low signal to noise scattering signal.

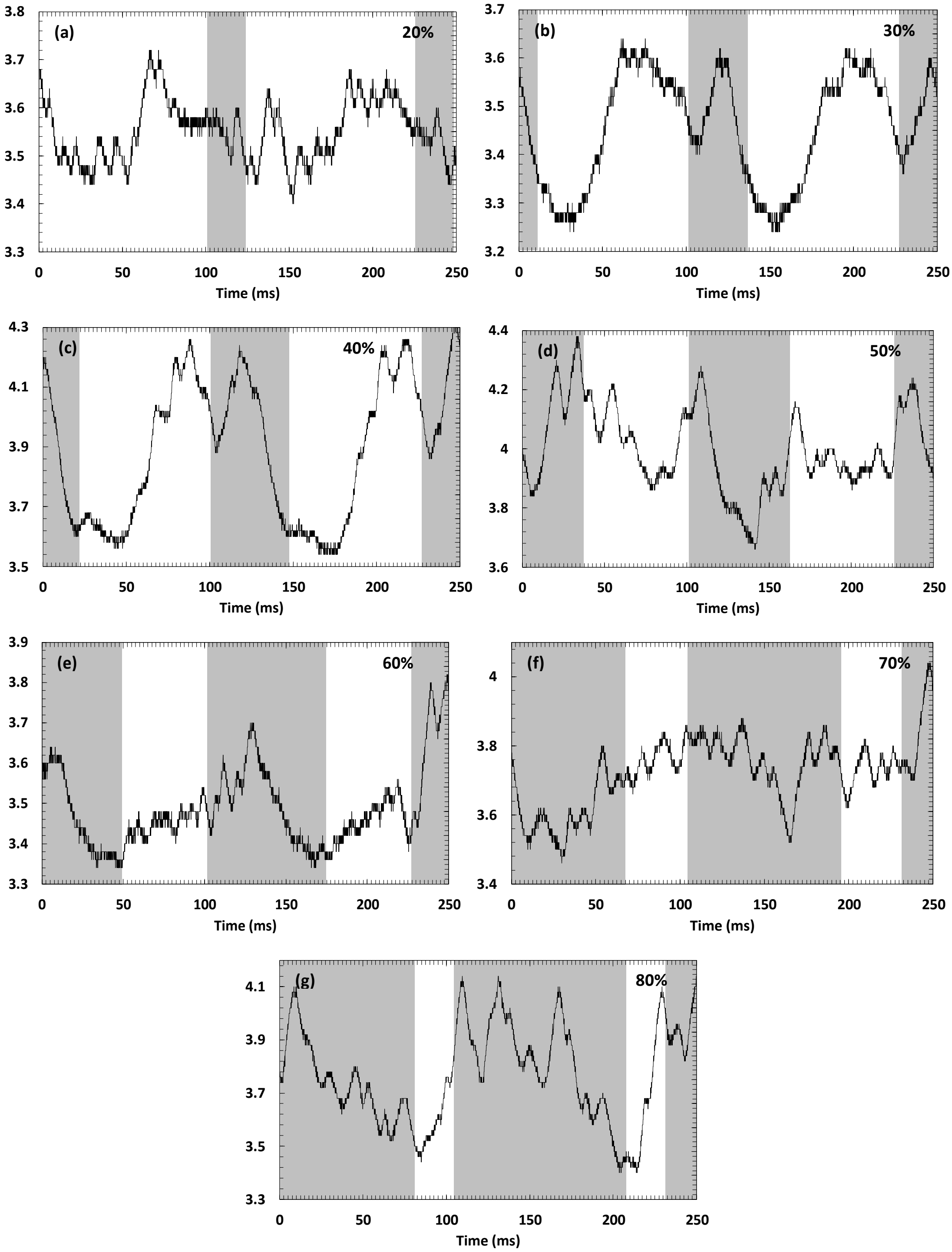

Figure 5.4: Unfocused random-AOS signal at 8 Hz pump for an off-resonant case.

5.3. Focused Pump Laser

After performing the unfocused resonant all-optical switching experiments and the off-resonance verification experiment, the lens was put back to observe the elastic scattering signal for the focused pump beam. The results of these experiments are plotted in figure 5.5. However the frequency was slightly changed for this experiment to 7 Hz to change the total on and off time for one cycle to 142 ms. Figure 5.5 (f) is the prime example of the type of switching achieved with this experiment, where the signal goes up in the on time with the change of refractive index, and comes down, i.e., reverts back to its original value in the off time. Table 5.1 shows the comparison between the focused and unfocused pump laser parameters.

Parameter	Units	Unfocused	Focused
Pump Power	mW	7.8	6.32
Beam Diameter	cm	0.24	0.017
Spot Area	cm^2	0.0452	0.0002
Pump Intensity	mW/cm^2	172	27844
Operating Frequency	Hz	7	7
Pump On Duration	ms	115	115
Pump Energy	mJ	0.16	0.73

Table 5.1: Unfocused and focused pump laser parameters comparison.

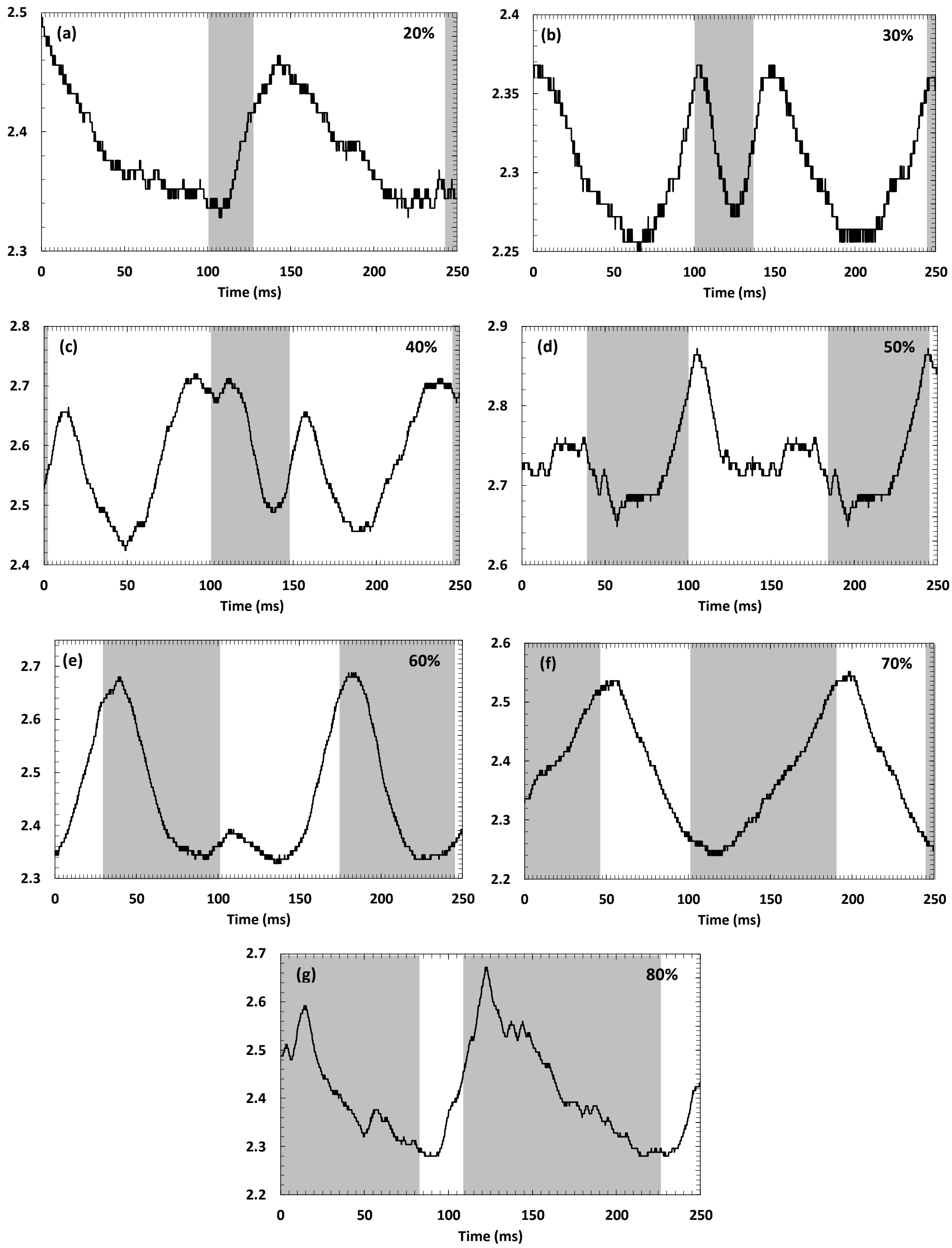

Figure 5.5: Focused AOS signal for a 7 Hz pump operating at 14.6ºC probe.

5.4. Detailed timing signal for duty cycles from 10% to 90%

After performing experiments with a focused pump laser, another experiment was performed by using the focused output of the pump laser. The comparison between the focused and the unfocused pump laser is given in table 5.1. However, if the data for the focused and unfocused elastic light scattering spectra is compared, a visible difference can be observed on the vertical axes of the Figures 5.2 and 5.5, and in the unfocused data of Figure 5.2; the vertical axis showing the elastic light scattering signal has values as high as 8 V, however that is not the case for Figure 5.5, where a focused pump is used to illuminate the sphere, the highest value of the elastic scattering signal on Figure 5.5 is 2.7 V. However, it should be kept in mind that for all of these experiments the laser diode was being operated at a current of 23.5 mA, which is way below the current limit i.e., 27mA, therefore this effect observed is because of the focused and the unfocused pump lasers. For this experiment the electronic function generator was replaced with a function generator with the capability of generating duty cycles below and above 20% and 80%. More elastic scattering signal plots were recorded to further understand the effect of the pump laser on the elastic scattering spectra in time. Figure 5.6 shows the detailed plots of this experiment ranging from 10% duty cycle to 90%, with the time scale was increased from 250 ms to 500 ms wave. The same pattern as observed in Figures 5.2, 5.3 and 5.5 is again evident in these plots. However, better patterns are observed in Figures 5.5 (j), (k), (l) and (m) as the duty cycles for these plots are 45%, 50%, 53% and 55% respectively. Since these duty cycles correspond to the pump being almost half off and half for the total pulse durations, an almost equal and opposite pattern of the elastic scattering signal is observed, as in the on time the signal decreases and in the off time it increases i.e., the refractive index of the sphere is getting restored in the off instance.

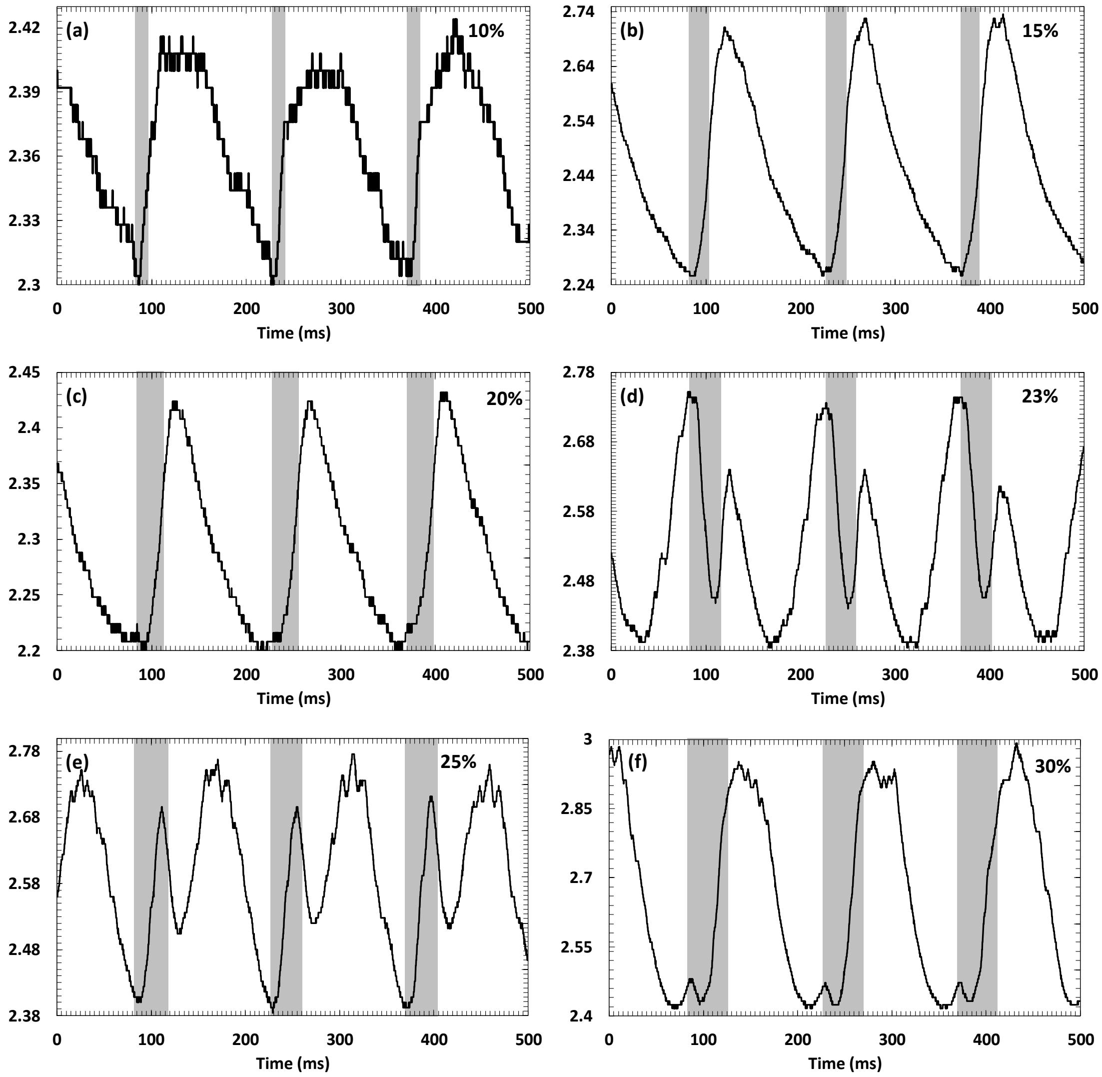

Figure 5.6: Focused AOS at 7 Hz pump at 15.4ºC probe for 10% to 90%.

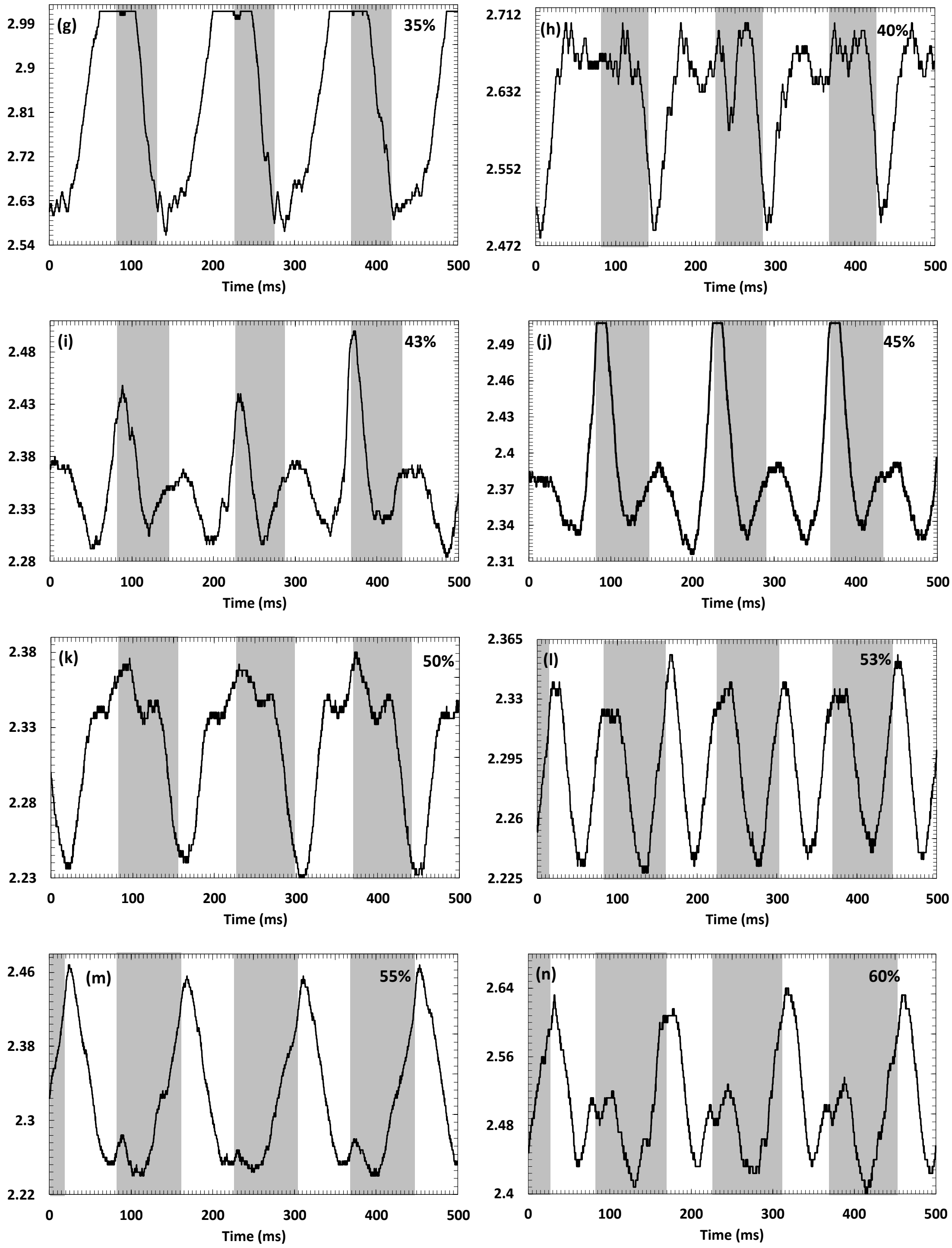

Figure 5.6: (Cont'd) Focused AOS at 7 Hz pump at 15.4ºC probe for 10% to 90%.

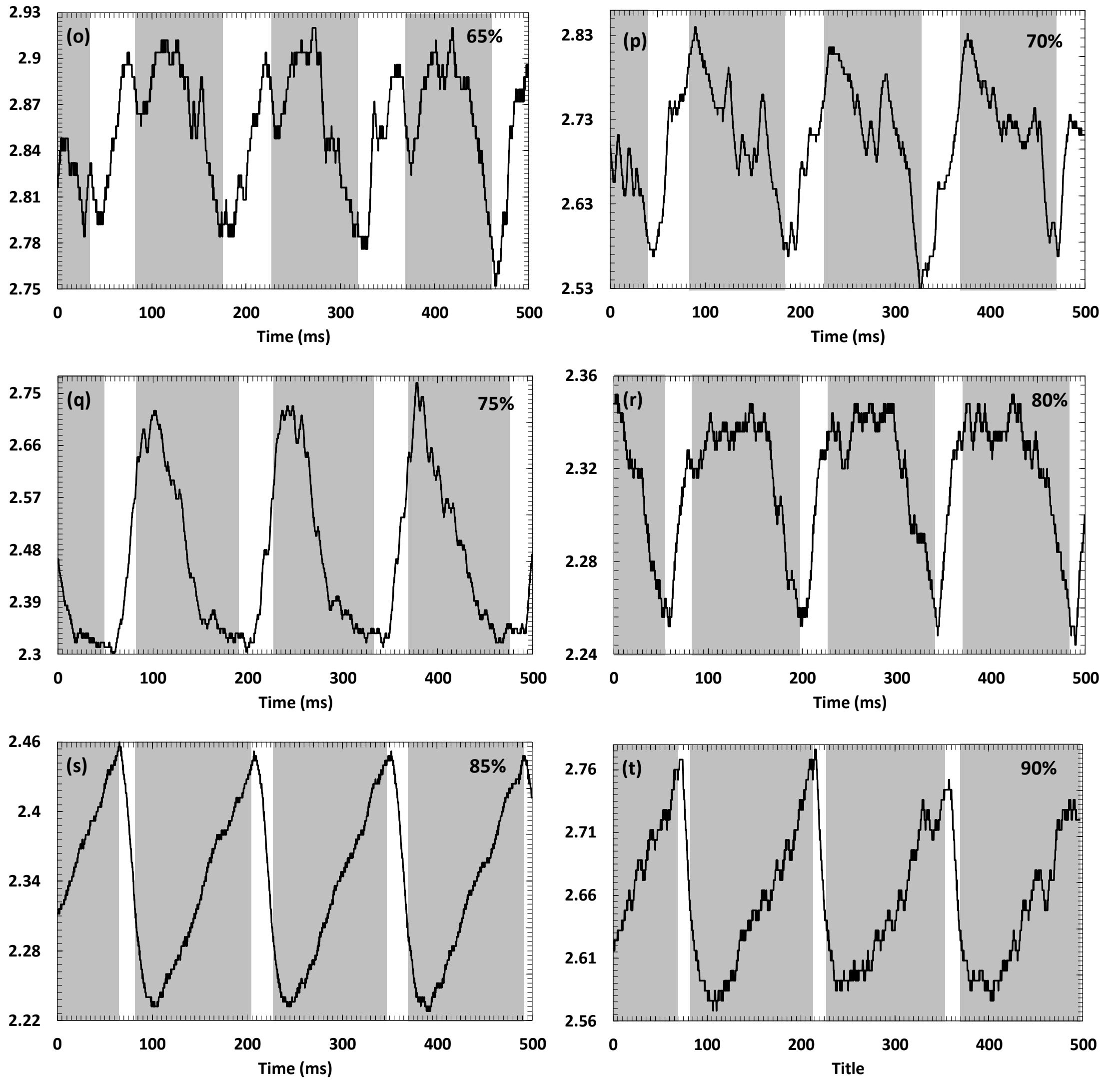

Figure 5.6: (Cont'd) Focused AOS at 7 Hz pump at 15.4ºC probe for 10% to 90%.

The comparison between Figures 5.5 (b) and (s) shows an exactly opposite pattern, as the plots are for the duty cycles of 15% and 85% respectively. 15% and 85%, duty cycles correspond to an approximately off pump laser and a continuous wave (CW) pump, therefore the effect of the pump of these duty cycles is absolutely opposite of each other.

Chapter 6

CONCLUSION

All-optical tuning was demonstrated in the transmission and scattering spectra of a silicon microsphere of 1 mm diameter and refractive index of 3.48 in the near-IR probe wavelength of 1472 nm. A 405 nm pump laser with pulsed output operating in the millisecond regime is used to control the resonances of the probe laser and an average shift of 0.37 nm for 50% duty cycle, which leads to an average refractive index change $\Delta N = 8.75 \times 10^{-4}$ and an average temperature change $\Delta T = 4.70$ K. Also, we demonstrated optical switching of silicon microsphere MDRs in the 90° elastic scattering with the help of TOE induced OPA for both focused and unfocused pump lasers.

These results can be used for optical modulators for semiconductor applications and can ultimately lead to all optical computing. For future work, a coupled pump source can be taken into account, as the pump in this study was a free space laser, a Y-coupler can be used to couple both the probe and the pump lasers into the OFHC. As this was one of the very first all-optical modulation studies in silicon microspheres, many other parameters can be changed in the future studies, such as the pump laser wavelength can be changed, as in this study a Fabry-Pérot 405 nm pump laser was used, an increased wavelength laser in the near-IR regime can be used to induce TPA. One of the very first all-optical control studies in silicon was conducted with a 532 nm laser, that can also be a possible choice for the pump laser for the all-optical control studies in silicon microspheres. The carrier lifetime in the silicon microsphere can be increased to observe a TPA induced FCD, and observe a blueshift instead of observing a redshift of the wavelength. The final experimental setup for this study did not include a lock-in amplifier, the scattering and the transmission data can be further refined and amplified using a lock-in amplifier. However, this study was conducted in the millisecond regime and at a frequency range of 7 to 8 Hz, the next step in this study can be to perform this study for high frequencies and at ultrafast regimes, for definite applciations in integrated photonics and photonics computing.

VITA

Farhan Azeem attended secondary school at Frontier Children Academy, Peshawar and graduated with a Secondary School Certificate in 2006. Later, he got accepted in F.Sc. Pre-Engineering in the prestigious Islamia University College, Peshawar and graduated with a Higher Secondary School Certificate in in 2008. Afterwards, he got accepted in the B.S. Telecommunication Engineering program at National University of Computer and Emerging Sciences (NUCES), Peshawar. He graduated from NUCES in 2012.

In 2013, he received Higher Education Commission (HEC) of Pakistan Scholarship and chose to pursue his graduate studies at Koç University, Istanbul after getting accepted in M.Sc. Optoelectronics and Photonics Engineering program as a teaching and research assistant. He joined Koç University Microphotonics Research Laboratory led by Prof. Dr. Ali Serpengüzel.

During his study in Koç University Microphotonics Research Laboratory, he worked on silicon microspheres and their applications in optoelectronics and photonics.

BIBLIOGRAPHY

1. L. Rayleigh, “The problem of the whispering gallery,” Scientific Papers **5**, 617-620 (1912).

2. G. Mie, “Contribution to the optical properties of turbid media, in particular of colloidal suspensions of metals,” Ann. Phys **25**, 377-452 (1908).

3. A. Serpengüzel, G. Griffel, and S. Arnold, "Excitation of resonances of microspheres on an optical fiber," Opt. Lett. **20**, 654-656 (1995)

4. K. J. Vahala, “Optical Microcavities,” World Scientific, Singapore (2004).

5. A. Serpengüzel, S. Arnold, G. Griffel, and J.A. Lock, “Enhanced coupling to microsphere resonances with optical fibers,” J. Opt. Soc. Am. B **14**, 790-795 (1997).

6. A. Chiasera, Y. Dumeige, P. Féron, M. Ferrari, Y. Jestin, G. Nunzi Conti, S. Pelli, S. Soria, and G.C. Righini, “Spherical whispering-gallery-mode microresonators,” Laser Photon. Rev. **4**, 457-482 (2010).

7. Y. Panitchob, G. Senthil Murugan, M. N. Zervas, P. Horak, S. Berneschi, S. Pelli, G. Nunzi Conti, and J. S. Wilkinson, “Whispering gallery mode spectra of channel waveguide coupled Microspheres,” Opt. Express **16**, 11066-11076 (2008).

8. Ch. Fabry and A. Pérot, “Theorie et applications d'une nouvelle methode de spectroscopie interferentielle, ” Ann. Chim. Phys. **16**, 115-144, (1899).

9. N. Vukovic, N. Healy, P. Horak, J. R. Sparks, P.J.A. Sazio, J. B. Badding, and A. C. Peacock, "Ultra-smooth microcylindrical resonators fabricated from the silicon optical fiber platform," Appl. Phys. Lett. **99**, 031117-1-031117-3 (2011).

10. L. Zhou and A.W. Poon, "Silicon electro-optic modulators using p-i-n diodes embedded 10-micron-diameter microdisk resonators," Opt. Express **14**, 6851-6857 (2006).

11. S. Feng, X. Luo, S. Du, and A.W. Poon, "Electro-optical tunable time delay and advance in a silicon feedback-microring resonator," Opt. Lett. **36**, 1278-1280 (2011).

12. W.D. Sacher and J.K.S. Poon, "Dynamics of microring resonator modulators," Opt. Express **16**, 15741-15753 (2008).

13. D. Armani, B. Min, A. Martin, and K. J. Vahala, "Electrical thermo-optic tuning of ultrahigh-Q microtoroid resonators," Appl. Phys. Lett. **85**, 5439-(2004).

14. A. Serpengüzel, G. Griffel, and S. Arnold, "Excitation of resonances of microspheres on an optical fiber," Opt. Lett. **20**, 654-656 (1995).

15. K. Srinivasan, P. E. Barclay, O. Painter, J. Chen, A. Y. Cho, and C. Gmachl, "Experimental demonstration of a high quality factor photonic crystal microcavity," Appl. Phys. Lett. **83**, 1915-1917 (2003).

16. S. C. Hill, A. C. Hill and P. W. Barber, "Light scattering by size/shape distributions of soil particles and spheroids," Appl. Opt. **23**, 1025-1031 (1984).

17. V.S. Ilchenko, M.L. Gorodetsky, X.S. Yao, and L. Maleki, "Microtorus: a high-finesse microcavity with whispering-gallery modes," Opt. Lett. **26**, 256-258 (2001).

18. M. Cai, O. Painter and K. J. Vahala, "Observation of critical coupling in a fiber taper to a silica-microsphere whispering-gallery mode system," Phys. Rev. Lett. **85**, 74-77 (2000).

19. D. W. Vernooy, V. S. Ilchenko, H. Mabuchi, E. W. Streed and H. J. Kimble, "High-Q measurements of fused-silica microspheres in the near infrared," Opt. Lett. **23**, 247-249 (1998).

20. G. R. Elliott, D. W. Hewak, G. S. Murugan, and J. S. Wilkinson, "Chalcogenide glass microspheres; their production, characterization and potential," Opt. Express **15**, 17542-17553 (2007).

21. P. Wang, T. Lee, M. Ding, A. Dhar, T. Hawkins, P. Foy, Y. Semenova, Q. Wu, J. Sahu, G. Farrell, J. Ballato, and G. Brambilla, "Germanium microsphere high-Q resonator," Opt. Lett. **37**, 728-730 (2012).

22. A. Serpengüzel, "Silicon microspheres," Proc. SPIE 6101, Laser Beam Control and Applications, **61010K** (2006).

23. G. Masini, L. Colace and G. Assanto, "Si based optoelectronics for communications," Mater. Sci. Eng. B **89**, 2-9 (2002).

24. H.C. Ren, F. Vollmer, S. Arnold and A. Libchaber, “High-Q microsphere biosensor-analysis for adsorption of rodlike bacteria,” Opt. Express **15**, 17410-17422 (2007).

25. M. S. Murib, W. S. Yeap, D. Martens, P. Bienstman, W. De Ceuninck, B. van Grinsven, M. J. Schöning, L. Michiels, K. Haenen, M. Ameloot, A. Serpengüzel and P. Wagner, “Photonic detection and characterization of DNA using sapphire microspheres,” J. Biomedical Opt. **19,** 097006-1 - 097006-7 (2014).

26. E. Yüce, O. Gürlü, and A. Serpengüzel, “Optical Modulation with Silicon Microspheres,” IEEE Photon. Technol. Lett. **21**, 1481-1483 (2009).

27. C. Tapalian, J. P. Laine, and P. Lane, “Thermooptical switches using coated microsphere resonators,” IEEE Photon. Technol. Lett.**14**, 1118–1120 (2002).

28. C. A. Mack, “Fifty Years of Moore’s Law,” IEEE Transactions Semiconductor Manufacturing. **24**, 202-207 (2011).

29. T.H. Ning, “Silicon technology directions in the new millennium,” in Proceedings of 38th Annual 2000 IEEE International Conference on Reliability Physics Symposium, 1-6 (2000).

30. R. Soref, “The Past, Present, and Future of Silicon Photonics,” IEEE J. Sel. Top. Quantum Electron. **12**, 1678-1687 (2006).

31. B. Jalali and S. Fathpour, “Silicon Photonics”, J. Lightwave Technol. **24**, 4600-4615 (2006).

32. S. Fathpour and B. Jalali, eds., Silicon Photonics for Telecommunications and Biomedicine (CRC Press, 2012).

33. O. Wada, “Femtosecond all-optical devices for ultrafast communication and signal processing,” New J. Phys. **6**, 183 (2004).

34. Y. O. Yılmaz, A. Demir, A. Kurt, and A. Serpengüzel, “Optical channel dropping with a silicon microsphere,” IEEE Photon. Technol. Lett. **17**, 1662–1664 (2005).

35. X. Li, A. Pyatenko, Y. Shimizu, H. Wang, K. Koga, and N. Koshizaki, “Fabrication of crystalline silicon spheres by selective laser heating in liquid medium,” Langmuir **27**, 5076–5080 (2011).

36. L. Shi, R. Fenollosa, T. U. Tuzer, and F. Meseguer, “Angle dependent quality factor of Mie resonances in silicon colloid-based microcavities,” ACS Photon. **1,** 408-412 (2014).

37. G. Cocorullo, M. Iodice, I. Rendina and P. M. Sarro, “Silicon thermooptical micromodulator with 700-kHz -3-dB bandwidth,” IEEE Photonics Technology Letters. **7**, 363-365 (1995).

38. G. Cocorullo, M. Iodice, I. Rendina, and P. M. Sarro, “All-silicon thermo-optic micro-modulator.” in IEEE Proceedings of the 25th European Solid State Device Research Conference, ESSDERC'95, 651-654 (1995).

39. L. L. Martín, C. Pérez-Rodríguez, P. Haro-González, and I. R. Martín, "Whispering gallery modes in a glass microsphere as a function of temperature," Opt. Express **19**, 25792-25798 (2011)

40. G. T. Reed, G. Mashanovich, F. Y. Gardes and D. J. Thomson, "Silicon optical modulators." Nature photonics **4**, 518-526 (2010).

41. Q, Xu, B. Schmidt, S. Pradhan, and M. Lipson, "Micrometre-scale silicon electro-optic modulator," Nature **435**, 325-327 (2005).

42. E. Yüce, O. Gürlü, G. J. Thursby and A. Serpengüzel, "Dynamical electrical tuning of a silicon microsphere: used for spectral mapping of the optical resonances," Applied Optics, **53**, 6181-6184 (2014).

43. E. Yüce, M. S. Murib, O. Gürlü and A. Serpengüzel, "Silicon microspheres for optical modulation applications," Photonic Materials, Devices, and Applications III, Volume **7366**, 73660O (2009).

44. A. Serpengüzel, A. Kurt, and U. K. Ayaz, "Silicon microspheres for electronic and photonic integration," Photon. Nanostr. Fundam. Appl. **6**, 179–182 (2008).

45. R. Normandin, D. C. Houghton and M. Simard-Normandin, "All-optical, silicon based, fiber optic modulator using a near cutoff region," Canadian Journal of Physics **67**, 412-419 (1989).

46. S. Stepanov and S. Ruschin, "Modulation of light by light in silicon-on-insulator waveguides," Applied Physics Letters **83**, 5151-5153 (2003).

47. R. Jones, A. Liu, H. Rong, M. Paniccia, O. Cohen and D. Hak, “Lossless optical modulation in a silicon waveguide using stimulated Raman scattering,” Opt. Express **13**, 1716-1723 (2005).

48. V. R. Almeida, C. A. Barrios, R. R. Panepucci, M. Lipson, M. A. Foster, D. G. Ouzounov, and A. L. Gaeta, “All-optical switching on a silicon chip,” Opt. Lett. **29**, 2867-2869 (2004).

49. V. R. Almeida, C. A. Barrios, R. R. Panepucci and M. Lipson, “All-optical control of light on a silicon chip,” Nature **431**, 1081-1084 (2004).

50. K. Ogusu, and K. Shinkawa, “Optical nonlinearities in silicon for pulse durations of the order of nanoseconds at 1.06 μm,” Opt. Express **16**, 14780-14791 (2008).

51. L. W. Luo, G. S. Wiederhecker, K. Preston and M. Lipson, “Power insensitive silicon microring resonators,” Opt. Lett. **37**, 590-592 (2012)

52. G. Cocorullo and I. Rendina, “Thermo-optical modulation at 1.5 μm in silicon etalon.” Electronic. Lett. **28**, 83-85 (1992).

53. V. R. Almeida and M. Lipson, “Optical bistability on a silicon chip,” Opt. Lett. **29**, 2387-2389 (2004)

54. Y. Su, F. Liu, Q. Li, Z. Zhang and M. Qiu, “System performance of slow-light buffering and storage in silicon nano-waveguide,” Proc. SPIE on Optical Transmission, Switching, and Subsystems V**6783**, 67832P (2007).

55. A. Martínez, J. Blasco, P. Sanchis, J. V. Galán, J. García-Rupérez, E. Jordana, P. Gautier, Y. Lebour, S. Hernández, R. Spano, R. Guider, N. Daldosso, B. Garrido, J. M. Fedeli, L. Pavesi, and J. Martí, “Ultrafast All-Optical Switching in a Silicon-Nanocrystal-Based Silicon Slot Waveguide at Telecom Wavelengths,” Nano Letters **10** (4), 1506-1511 (2010)

56. K. Ikeda, R. E. Saperstein, N. Alic, and Y. Fainman, “Thermal and Kerr nonlinear properties of plasma-deposited silicon nitride/ silicon dioxide waveguides,” Opt. Express **16**, 12987-12994 (2008).

57. H.C. Tapalian, J. P. Laine, P.A. Lane, “Thermooptical switches using coated microsphere resonators,” IEEE Photonics Technology Letters **14**, 1118-1120 (2002).

58. A. Tewary, M. J. F. Digonnet, M. L. Brongersma, J. Y. Sung and J. H. Shin, “Silicon-nanocrystal-coated silica microsphere thermooptical switch,” Proc. SPIE on Silicon Photonics **6125**, 61250U (2006).

59. P. Wang, M. Ding, T. Lee, G. S. Murugan, L. Bo, and Y. Semenova, Q. Wu, D. Hewak, G. Brambilla, and G. Farrell, “Packaged chalcogenide microsphere resonator with high Q-factor,” Applied Physics Letters **102**, 131110 (2013) .

60. C. A. Lin, J. H. Chen and L. A. Wang, “High- Q Si Microsphere Resonators Fabricated From Si-Cored Fibers for WGMs Excitation,” IEEE Photonics Technology Letters **27**, 1355-1358 (2015).

61. M. Biancardo, K. Taira, N. Kogo, H. Kikuchi, N. Kumagai, N. Kuratani, I. Inagawa, S. Imoto and J. Nakata, “Characterization of microspherical semi-transparent solar cells and modules,” Solar Energy **81**, 711-716 (2007).

62. M. Garín, R. Fenollosa, R. Alcubilla, L. Shi, L. F. Marsal, and F. Meseguer, “All-silicon spherical-Mie-resonator photodiode with spectral response in the infrared region,” Nature Communications **5**, 3440 (1-6) (2014).

63. Q. Shabir, A. Pokale, A. Loni, D. R. Johnson, L. T. Canham, R. Fenollosa and M. Tymczenko, “Medically biodegradable hydrogenated amorphous silicon microspheres,” Silicon **3**, 173-176 (2011).

64. F. Ramiro-Manzano, R. Fenollosa, E. Xifré-Pérez, M. Garín, and F. Meseguer, “Porous silicon microcavities: synthesis, characterization, and application to photonic barcode devices,” Nanoscale Research Lett. **7**, 1-6 (2012).

65. U. S. Gökay, M. Zakwan, and A. Serpengüzel, “Spherical silicon optical resonators: Possible applications to biosensing,” The European Physical Journal Special Topics **223**, 2003-2008 (2014).

66. M. H. Humayun, F. Azeem, I. Khan, U. S. Gökay, and A. Serpengüzel, “Silicon Microspheres in Metrology,” Proceedings of the PIERS, 215 (2015).

67. A. F. Oskooi, D. Roundy, M. Ibanescu, P. Bermel, J. D. Joannopoulos, and S. G. Johnson, “MEEP: A flexible free-software package for electromagnetic simulations by the FDTD method,” Computer Physics Communications, **181**, 687-702 (2010).

68. P. Chýlek, “Resonance structure of Mie scattering: distance between resonances”, J. Opt. Soc. Am. A **7**, 1609-1613 (1990).

69. P. W. Barber and S. C. Hill, “Light Scattering by Particles: Computational Methods”, World Scientific, Singapore (1990).

70. J. A. Lock and G. Gouesbet, “Generalized Lorenz-Mie theory and applications”, J. Quant Spectrosc. Radiat. Transfer **110**, 800-807 (2009).

71. P. Guillon and Y. Garault, “Accurate Resonant Frequencies of Dielectric Resonators,” IEEE Transactions on Microwave Theory and Techniques, **25**, 916-922, (1977).

72. M. S. Murib, E. Yüce, O. Gürlü, and A. Serpengüzel, “Polarization behavior of elastic scattering from a silicon microsphere coupled to an optical fiber,” Photonics Research **2**, 45-50, 2014.

73. J. P. Laine, C. Tapalian, B. Little, H. Haus, “Acceleration Sensor Based on High-Q Optical Microsphere Resonator and Pedestal Antiresonant Reflecting waveguide Coupler,” Sensors and Actuators A **93**, 1-7, (2001).

74. C. A. Barrios and M. Lipson, “Silicon Photonic Read Only Memory,” J. Lightwave Technol **24**, 7 (2006).

75. O. Boyraz, and B. Jalali: “Demonstration of a silicon Raman laser,” Opt. Exp., **12**, 5269-5273 (2004).

76. G. T. Reed and K. P. Andrew, “Silicon Photonics; An Introduction”, John Wiley and Sons Ltd., West Sussex (2004).

77. M. E. Castagna, S. Coffa, M. Monaco, A. Muscara, L. Caristia, S. Lorenti, and A. Messina, “High efficiency light emitting devices in silicon,” Materials Science and Engineering: B **105**, 83-90 (2003).

78. B. E. Saleh and M. C. Teich, “Fundamentals of photonics,” Vol. 22. New York: Wiley (1991).

79. P. Weinberger, “John Kerr and his effects found in 1877 and 1878,” Philosophical Magazine Letters **88**, 897-907 (2008).

80. R. A. Soref and B.A. Bennett, ‘’Electrooptical effects in Silicon,’’ IEEE J. Quantum Electron. **23**, 123 (1987).

81. X. Sang, E.K. Tien and O. Boyraz, “Applications of two-photon absorption in silicon,” J. Optoelectron. Advanced Materials **11**, 15-25 (2008).

82. X. Ma and G. Sheng, “Optical switching technology comparison: Optical MEMS vs. other technologies,” IEEE Optical Communications, s16-s23 (2003).